JOURNAL OF GEOPHYSICAL RESEARCH, VOL. 104, NO. D3, PAGES 3711-3727, FEBRUARY 20, 1999

# Space-time patterns of trends in stratospheric constituents derived from UARS measurements

William J. Randel and Fei Wu
National Center for Atmospheric Research, Boulder, Colorado

James M. Russell III
Hampton University, Hampton, Virginia

Joe Waters
Jet Propulsion Laboratory, Pasadena, California

**Abstract.** The spatial and temporal behavior of low-frequency changes (trends) in stratospheric constituents measured by instruments on the Upper Atmosphere Research Satellite (UARS) during 1991-98 is investigated. The data include $CH_4$, $H_2O$, HF, HCl, $O_3$, and $NO_2$ from the Halogen Occultation Experiment (HALOE), and $O_3$, ClO, and $HNO_3$ from the Microwave Limb Sounder (MLS). Time series of global anomalies are analyzed by linear regression and empirical orthogonal function analysis. Each of the constituents show significant linear trends over at least some region of the stratosphere, and the spatial patterns exhibit coupling between the different species. Several of the constituents (namely $CH_4$, $H_2O$, HF, HCl, $O_3$, and $NO_2$) exhibit a temporal change in trend rates, with strong changes prior to 1996 and weaker (or reversed) trends thereafter. Positive trends are observed in upper stratospheric ClO, with a percentage rate during 1993-97 consistent with stratospheric HCl increases and with tropospheric chlorine emission rates. Significant negative trends in ozone in the tropical middle stratosphere are found in both HALOE and MLS data during 1993-97, together with positive trends in the tropics near 25 km. These trends are very different from the decadal-scale ozone trends observed since 1979, and this demonstrates the variability of trends calculated over short time periods. Positive trends in $NO_2$ are found in the tropical middle stratosphere, and spatial coincidence to the observed ozone decreases suggests the ozone is responding to the $NO_2$ increase. Significant negative trends in $HNO_3$ are found in the lower stratosphere of both hemispheres. These coupled signatures offer a fingerprint of chemical evolution in the stratosphere for the UARS time frame.

## 1. Introduction

The Upper Atmosphere Research Satellite (UARS) was launched in September 1991 with a mission to observe a suite of chemical constituents of importance for stratospheric ozone (in addition to data on atmospheric dynamics and solar variability [*Reber,* 1993]). The UARS mission was originally projected to last for 18 months, with 1 year of extended operations. The satellite has now been operational for over 6 years, and two of the instruments designed for stratospheric constituent measurements are still providing data (namely the Halogen Occultation Experiment (HALOE) [*Russell et al.*, 1993] and the Microwave Limb Sounder (MLS) [*Barath et al.*, 1993]). The long time series of these constituent measurements provides an opportunity to study interannual variability in the chemical makeup of the stratosphere. In particular, these data provide information on monotonic low-frequency changes (trends) in the constituent fields, and the time series are now of sufficient length to study trend-like variability. The objective of this work is to quantify the spatial and temporal structure of these trends and to study the coherent behavior of the different constituents over the UARS time period.

The UARS HALOE data are analyzed here for the period covering October 1991 to July 1998; MLS data are analyzed through July 1997. We calculate linear trends over the period 1993-1997, omitting data from 1991-1992 because of possible effects of the Mt. Pinatubo eruption (in 1991) and strong changes in the solar cycle during this time. Five years is a relatively short time record to sample trend-like variability, much shorter than the ~ 16-18 year satellite records available to quantify column and profile ozone trends [e.g., *McPeters et al.*, 1996; *Stratospheric Processes and Their Role in Climate* (*SPARC*), 1998]. We thus examine both the linear trends over 1993-1997 and also details of the anomaly time series over the entire 1991-1998 record to quantify temporal variations (i.e., how linear are the trends). It turns out that almost all of the trends are very nonlinear, showing substantial changes in the latter part of the record (after 1996). Both the trends over 1993-1997 and the nonlinearity over the most recent part of the record show coherence between the various constituents. The observation of coherent low-frequency changes in several different species (many not previously available) provides several pieces to the puzzle of how the stratosphere evolves chemically on a decadal timescale.

Some of the results here extend prior trend analyses of the UARS data. *Russell et al.* [1996a] documented trends in



Paper number 1998JD100044.
0148-0227/99/1998JD100044$09.00

HALOE HF and HCl near the stratopause for data through early 1995, and the HF time series was extended to early 1997 by *Considine et al.* [1997]. *Nedoluha et. al.* [1998a,b] and *Evans et al.* [1998] reported trends in HALOE $H_2O$, $CH_4$, and $NO_2$, and *Siskind et al.* [1998] used model calculations to examine the sensitivity of $O_3$ and ClO trends to changes in these other species. Aspects of the HALOE and MLS ozone trends have been reported by *SPARC* [1998]. Further details of ClO trends from MLS measurements will be presented in "Long-term variations in the free chlorine content of the stratosphere" by L. Froidevaux et al. (hereinafter referred to as Froidevaux et al., manuscript in preparation, 1998). The objective here is to combine trend information on all the constituents into one location, using identical time intervals and statistical analyses, in order to derive a coherent picture of stratospheric variability.

## 2. Data

### 2.1. HALOE

The HALOE data analyzed here are from the version 18 (v18) retrieval algorithm, spanning the time period October 1991 to July 1998. The HALOE instrument is described by *Russell et al.* [1993], and details of the data are presented by *Park et al.* [1996], *Harries et al.* [1996], *Russell et al.* [1996b,c], *Bruhl et al.* [1996], and *Gordley et al.* [1996] for $CH_4$, $H_2O$, HF, HCl, $O_3$, and $NO_2$ data, respectively. We use HALOE level 3a data, available on 16 standard UARS pressure levels spanning 100-0.32 mb (approximately 16-56 km) with a vertical spacing of about 2.5 km. Sunrise and sunset HALOE measurements are combined for all constituents except $NO_2$ (which has a strong diurnal variation). We bin the data into monthly samples on a 4° latitude grid prior to the statistical analyses discussed below. Because HALOE does not observe polar regions during much of the year, we focus our results on the latitude band 60°N-S.

### 2.2. MLS

MLS observations of $O_3$, ClO, and $HNO_3$ are obtained from the version 4 (v4) retrieval algorithm. Details of the $O_3$ and ClO data (from v3 processing) are described by *Froidevaux et al.* [1996] and *Waters et al.* [1996], respectively. Changes to these constituents for v4, along with details of the $HNO_3$ data, are discussed partly in the above references and in the MLS 4 Data Quality Document (available from the MLS web site at http://mls.jpl.nasa.gov). We use MLS v4 level 3a data, for which retrievals are performed on the 100, 46, 22, 10, 4.6, 2.2, 1.0, and 0.46 mb pressure levels (every other UARS pressure level; vertical resolution ~ 5 km). The available data are binned into monthly samples on a 4° latitude grid. As a note, MLS data after June 1997 are somewhat different from earlier data, because MLS was then operating with only one radiometer. This may result in some small shifts in the data, and hence MLS data after June 1997 are not included in the trend analyses here.

Subsets of these vertical levels are analyzed here for each constituent (where the data are deemed "scientifically useful"). For $O_3$ and ClO, data over the 46-1 mb range are used, while for $HNO_3$, only the 100-, 46-, and 22-mb levels are analyzed. Additionally, for ClO (which has a strong diurnal variation), we bin separately the daytime and nighttime observations and analyze daytime data at 2.2 and 1.0 mb and day-night differences at and below 4.6 mb [after *Waters et al.*, 1996]. Individual profile data are screened, and only "QUALITY=4" profiles are included in the monthly means. We note that the availability of ClO data decreases substantially after 1994 and additionally that the ClO profile retrievals have relatively large noise uncertainties [*Waters et al.*, 1996].

### 2.3. SAGE II

Because we show ozone trends derived from HALOE and MLS data, it is of interest to directly compare trends calculated from the Stratospheric Aerosol and Gas Experiment II (SAGE II) ozone measurements over the same time period (1993-1997). SAGE II is a solar occultation instrument with similar space-time sampling to that for HALOE, but that makes observations in different spectral bands. We use the version 5.96 retrieval of SAGE II ozone, which incorporates improved separation of aerosol and ozone effects [*Cunnold et al.*, 1998]. These v5.96 SAGE II ozone data contribute a major role to the recent ozone trends evaluations by *SPARC* [1998] and *World Meteorological Organization* (WMO) [1998] (based on the SAGE II record over 1984-1996, and the SAGE I data over 1979-1981). The objective here is to examine SAGE II trends over the shorter period 1993-1997 for direct comparison to the HALOE and MLS results, and for comparison with the longer decadal changes.

## 3. Statistical Analyses

Previous analyses of HALOE data have shown clear evidence of low-frequency variations associated with (1) the seasonal cycle [e.g., *Luo et al.*, 1994; *Mote et al.*, 1996; *Randel et al.*, 1998] and (2) the quasi-biennial oscillation (QBO) [*Luo et al.*, 1996; *Randel et al.*, 1998]. Because both of these signals can be accurately characterized in an empirical manner, we remove them prior to examination of the data for "other" low-frequency variability. At each latitude and pressure level the seasonal cycle is fit using a seasonal harmonic analysis (with constant, annual and semiannual harmonics), while the QBO is fit using linear regression onto two orthogonal basis functions derived from the QBO equatorial zonal winds over 70-10 mb. The details of these statistical fits for $CH_4$ and $H_2O$ are shown by *Randel et al.* [1998]. Figure 1 shows an example of the procedure applied to $CH_4$ data at 3 mb over 16-24°N: the top panel shows the original data together with the seasonal cycle fit, and the middle panel shows the deseasonalized data and the statistical QBO fit. The bottom panel shows the corresponding residuals (full data minus seasonal and QBO fits), and these residuals are the basis for further analysis. Figure 1 includes a linear trend fit of these residuals (over 1993-1997) derived from standard regression analysis (extended with a dashed line through the entire 1991-1998 time series). We also remove "outliers" in the time series prior to trend (or empirical orthogonal function (EOF)) analyses by omitting residual data points with variations larger than 3 times the local temporal standard deviation.

Standard errors for the trend analyses are estimated using a bootstrap resampling of the original data [*Efron and Tibshirani*, 1993]. We sample 6-month segments of the data to automatically include the effect of serial autocorrelation. Significant trends (values larger than twice the statistical standard error) are indicated with shading in the contour plots of trends throughout this paper, note these estimates only account for statistical uncertainty and do not include any instrumental drift uncertainty. A further consideration when evaluating field statistics (such as trends over the latitude-height plane) is that even for completely random data, 5% of the samples would be "significant" based on

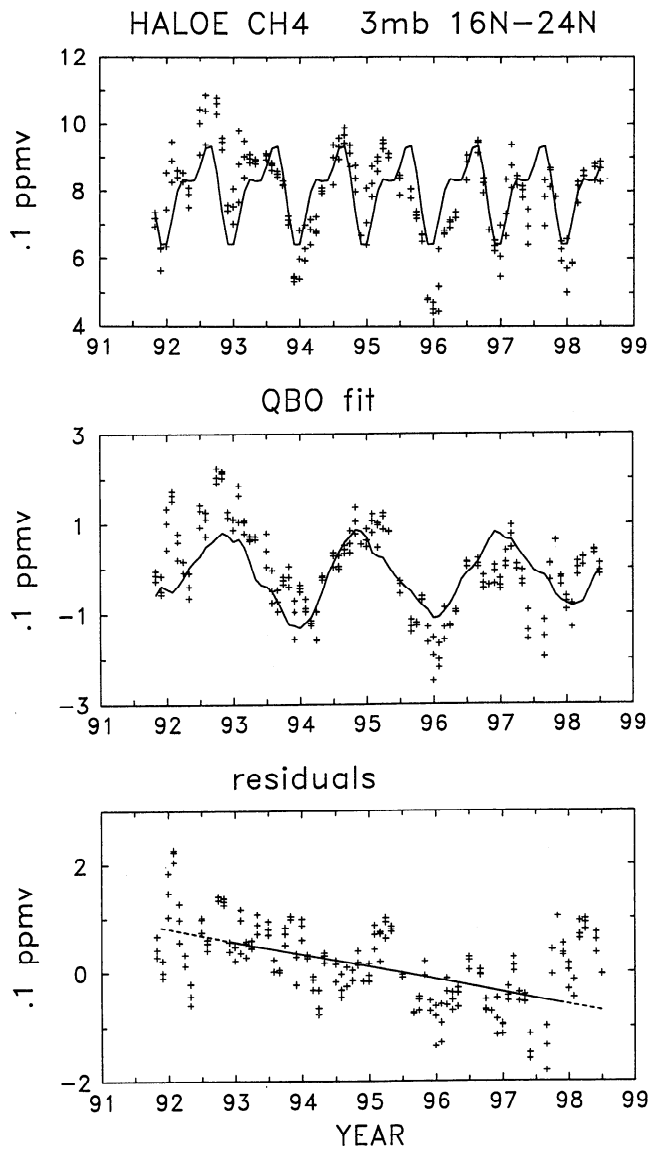


**Figure 1.** Time series of HALOE $CH_4$ data at 3 mb over 16-24°N. Top panel shows 'full' monthly means plus (repeating) seasonal cycle fit, while the middle panel shows the deseasonalized data plus the QBO regression fit. Bottom panel shows residual anomalies ('full' field minus seasonal and QBO fits), plus the linear trend (fit over 1993-97, and extended with a dashed line over 1991-98).

just random chance. However, the trend patterns identified here typically cover much more than 5% of the total area and (more importantly) exhibit spatial coherence and interrelationships between species that is suggestive of true geophysical variability.

All of the statistical fits here are made using time series over 1993-1997 only, because of possible anomalies during 1991-1992 due to Pinatubo aerosols (either true atmospheric structure or data retrieval problems). Relatively large anomalies during 1991-1992 that would affect trend results are seen in $O_3$ and $HNO_3$ data, for example. The 1991-1992 period is also associated with high solar cycle index, as shown in Figure 2, whereas there is a relative minimum over 1993-1997 (enhanced solar activity will lead to true atmospheric changes, and the high sunspot activity may affect some of the HALOE solar occultation measurements). Although the statistical analyses are calculated over 1993-1997 only, time series of anomalies (seasonal and QBO effects removed) are shown for the full 1991-1998 data. We often show time series of latitudinally averaged anomalies on specific pressure levels (e.g., hemispheric or global means) calculated by simple area averaging; for months when less than 50% of the particular region is sampled, the corresponding area mean is omitted in these time series.

Besides linear trend analysis, we use empirical orthogonal function (EOF) analysis in an attempt to isolate the dominant space and timescales of variability. EOF analysis is based on an eigenvector decomposition of the temporal covariance matrix [e.g., *Kutzbach*, 1970] and identifies modes of variability that explain optimal fractions of space-time variance. The mixing ratio anomaly covariances are area (cosine (latitude)) weighted prior to eigenanalysis. Output of the EOF analysis include eigenvalues (proportional to the fraction of total variance explained) and spatial structure of the modes; time variation is examined by projection of the original anomalies onto these spatial structures. These time projections illustrate the global time variations of the constituent anomalies integrated over latitude and height, spatially weighted by the structure of the EOF patterns. The EOF analysis allows independent estimation of coherent time variability in the data, allowing a search for a time-varying trend, for example.

## 4. Results

### 4.1. $CH_4$ and $H_2O$

The overall structure and variability of $CH_4$ and $H_2O$ are tightly coupled in the stratosphere, because $CH_4$ oxidation is a principal source of stratospheric $H_2O$ [e.g., *Remsberg et al.*, 1984]. The oxidation reactions produce approximately two molecules of $H_2O$ for each one of $CH_4$. Empirical studies of HALOE and other data sets have shown that the quantity $D = H_2O + 2CH_4$ is an approximately conserved parameter throughout much of the stratosphere [*Remsberg et al.*, 1984; *Dessler et al.*, 1994; *Remsberg et al.*, 1996]. We thus examine the variability of $CH_4$, $H_2O$ and $H_2O + 2CH_4$.

Figure 3 shows time series of hemispheric mean $CH_4$ anomalies in the lower stratosphere (31 mb, ~ 24 km) and near

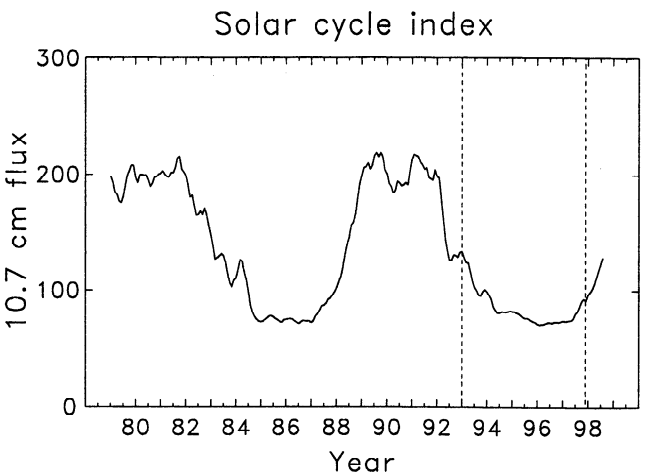


**Figure 2.** Time series of 10.7 cm solar flux, illustrating the 11-year solar cycle. The dashed lines indicate the time period covered by the trend calculations here (1993-97).

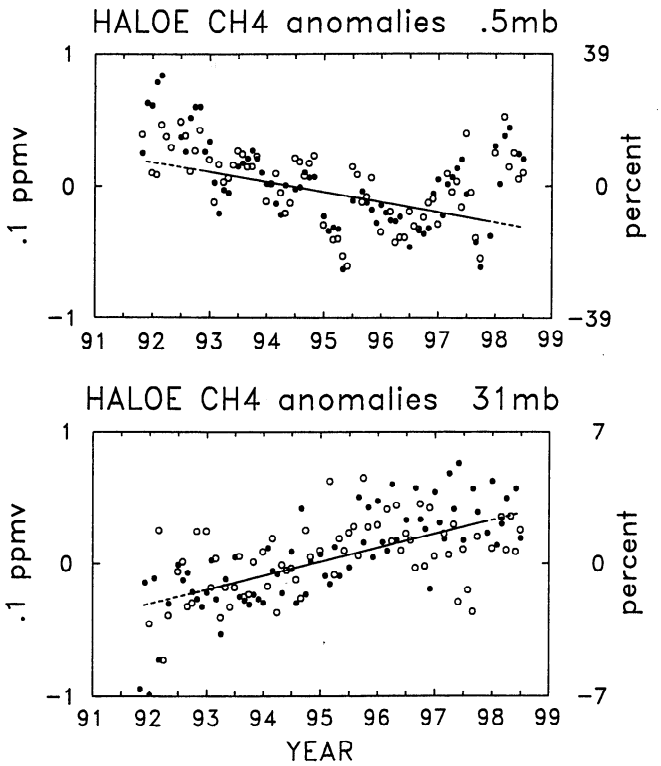


**Figure 3.** Time series of hemispheric $CH_4$ anomalies at 0.5 mb (top) and 32 mb (bottom). Solid and open circles denote NH and SH data, respectively. Straight lines are the regression-fit trends over 1993-97. The right hand axes indicate the approximate percentage variations, calculated as a fraction of the long-term means.

the stratopause (0.5 mb, ~ 53 km). The lower stratosphere anomalies show monotonic increase in time. In the upper stratosphere, $CH_4$ shows a clear decrease during 1992-1996, and then a reversal of the downward trends during 1997-1998; the most recent values are similar to those at the beginning of the record. The linear trends account for a large fraction of variance in these data during 1993-1997. Figure 4a shows a meridional cross section of trends in $CH_4$ over 1993-1997 in units of percent per year (relative to the local time mean values). Figures 4b and 4c show corresponding trend estimates for $H_2O$ and $H_2O + 2CH_4$, respectively. Positive $CH_4$ trends are seen in Figure 4a throughout the lower stratosphere with magnitude ~ + 1% per year; the global mean trend over 100-22 mb is 0.86 ± 0.40% per year (2 standard error uncertainty), and this is in reasonable agreement with measured $CH_4$ trends in the troposphere of ~ 0.7% per year calculated from data over 1983-1992 by *Dlugokencky et al.* [1994]. Significant negative $CH_4$ trends are observed in the upper stratosphere (≥ 40 km) in Figure 4a, with maximum values near the stratopause of –3 to –5% per year. A mixed $CH_4$ trend signal is observed in Figure 4a in the middle stratosphere (~ 30-40 km), with negative trends in the NH and weak or positive trends in the SH (with a relative maximum over 10°-30° near 40 km). This NH-SH asymmetry is also observed in the ~ 20-30 km layer, with positive NH trends that are larger and more significant than those in the SH.

Time series of hemispheric mean $H_2O$ anomalies at 10 mb and 1 mb are shown in Figure 5. These data show an overall increase throughout 1991-1996 but more constant values (or decreasing at 1 mb) for the more recent observations. Note the strong anticorrelation between the 1-mb $H_2O$ anomalies in Figure 5 and the 0.5-mb CH4 data in Figure 3; these are ratioed such that $H_2O + 2CH_4$ is approximately constant since 1996. The increase in stratospheric $H_2O$ in HALOE data prior to 1997 has been reported by *Nedoluha et al.*[1998a], who find similar upward

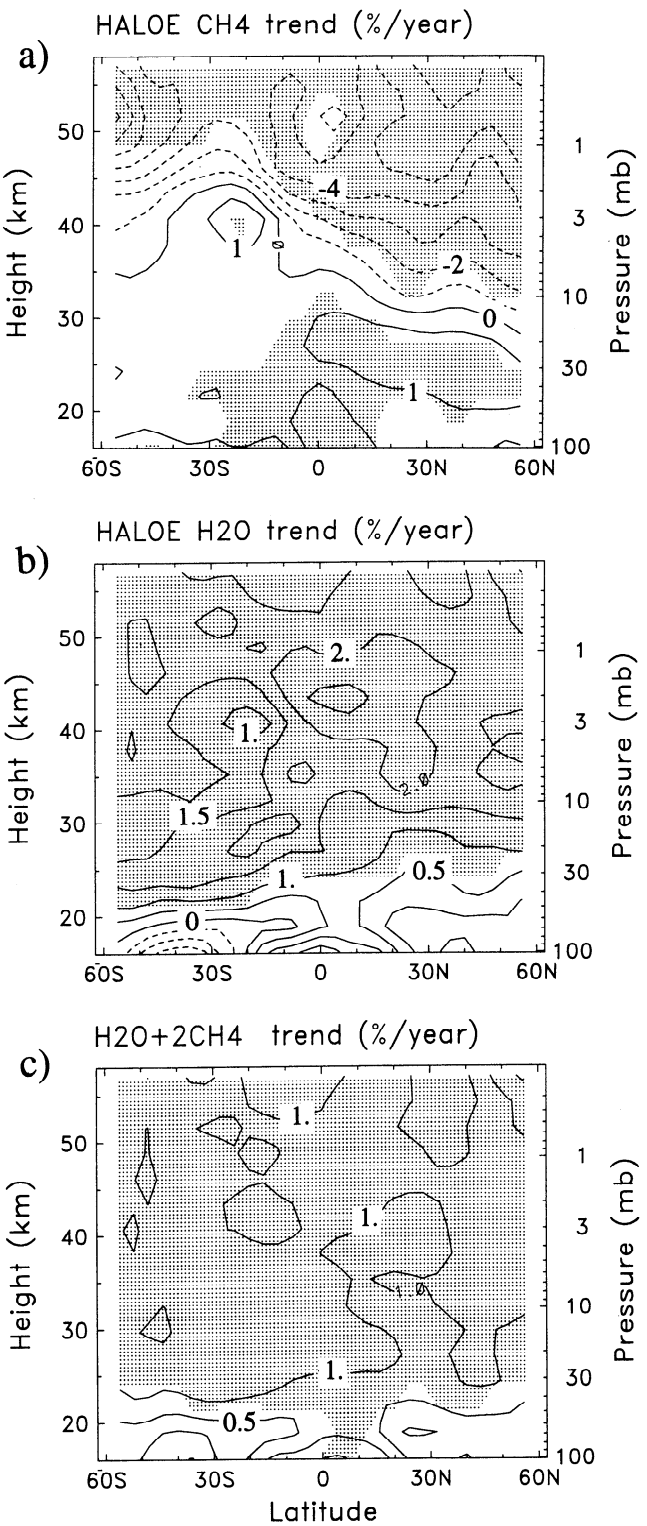


**Figure 4.** Meridional cross sections of linear trends in (a) $CH_4$, (b) $H_2O$, and (c) $H_2O + 2CH_4$. Trends are expressed in terms of local percentages (with respect to the long term means). Shading indicates the trends are statistically significant at the 95% (two sigma) level.

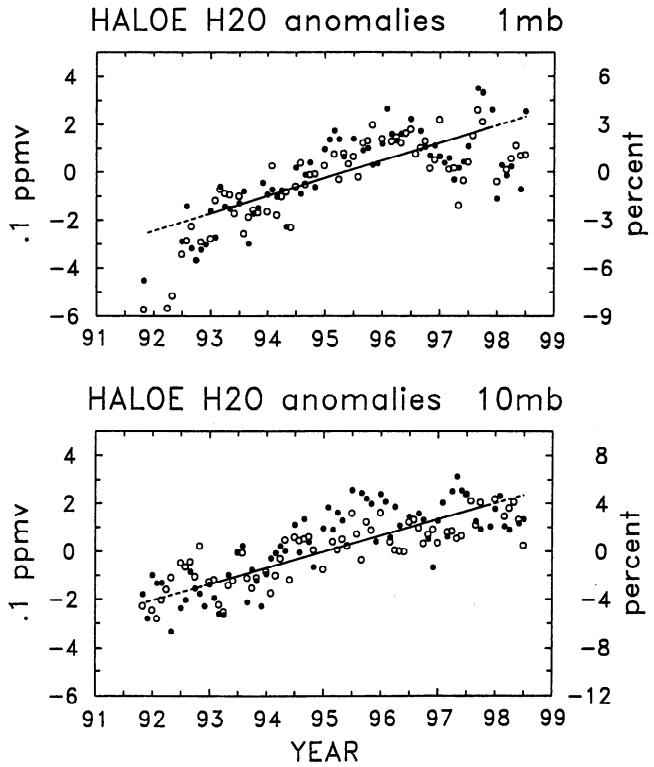


**Figure 5.** Time series of hemispheric $H_2O$ anomalies at 1 mb (top) and 10 mb (bottom), for NH (solid) and SH (open circles) observations, along with the 1993-97 trend fits.

trends in ground-based millimeter-wave spectrometer measurements. Figure 4b shows the HALOE $H_2O$ trends over 1993-1997 expressed in percent per year of the time-mean background. Positive trends of order 1-2% per year are found over most of the stratosphere above approximately 25 km; significant trends are not found below 20 km. *Oltmans and Hofmann* [1995] report significant trends in $H_2O$ during 1981-1994 at Boulder, Colorado (40°N) with magnitude ~ 0.4-0.8% per year over altitudes of 16-24 km, but significant trends are not seen in the zonal average HALOE v18 data (during 1993-1997) over these altitudes. As a note, the HALOE v18 $H_2O$ data below 20 km are less reliable than those above this altitude because of instrumental pointing uncertainties.

There is some spatial structure of note in the $H_2O$ trends, namely a minimum over 0°-30°S near 40 km, and an NH-SH asymmetry over ~ 23-30 km (with stronger positive trends in the SH than in the NH). These spatial patterns have strong correspondence to structure seen in the $CH_4$ trends (Figure 4a), such that their effects nearly cancel when trends in the quantity $H_2O + 2CH_4$ are calculated. As shown in Figure 4c, these trends exhibit less spatial structure than either $CH_4$ or $H_2O$ alone, with near constant trends (~ 1% per year) over the entire altitude range 20-55 km.

The altitude structure of the global mean trends in $CH_4$, $H_2O$, and $H_2O + 2CH_4$ are shown in Figure 6. Here the trends are expressed in units of mixing ratio tendencies (ppmv per year). This illustrates the relatively small contribution of the $CH_4$ trends to the total $H_2O + 2CH_4$, particularly in the upper stratosphere (although the percentage $CH_4$ trends are large in this region because of small background $CH_4$ levels). Physically, this means that the negative $CH_4$ trends in the upper stratosphere do not contribute a large fraction of the observed increase in $H_2O$ via oxidation, but rather there is an independent mechanism for the stratospheric $H_2O$ increases (as noted by *Nedoluha et al.* [1998a] and *Evans et al.* [1998]).

The application of EOF analysis to the HALOE $CH_4$, $H_2O$, and $H_2O + 2CH_4$ anomalies results in one predominant space-time variance structure (or mode) for each quantity (termed EOF1), and these each turn out to be closely related to the linear trends. Figure 7 shows the spatial structure of EOF1 for $CH_4$ and $H_2O$, and comparison with the respective trends (Figure 4) shows similar spatial patterns in both cases. The EOF1 spatial structure for the quantity $H_2O + 2CH_4$ (not shown) shows a broad spatial

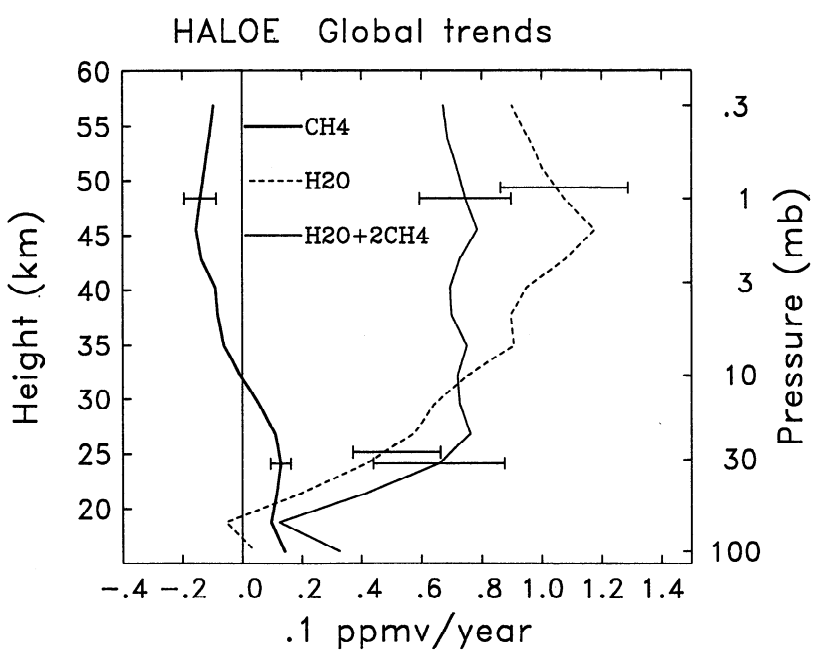


**Figure 6.** Altitude profiles of near global (60°N-S) trends in $CH_4$, $H_2O$ and $H_2O + 2CH_4$, expressed in terms of ppmv per year. Error bars show the respective two sigma uncertainties at 32 and 1 mb.

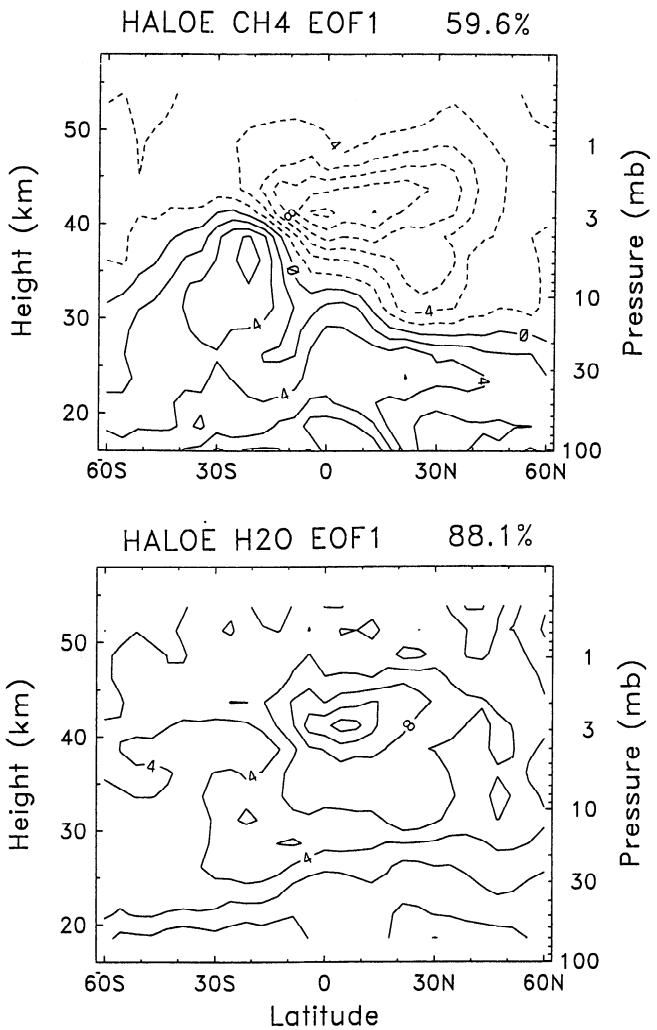


**Figure 7.** Meridional cross sections of the spatial structure of EOF1 for anomaly time series of $CH_4$ (top) and $H_2O$ (bottom). The percentage of total variance explained by EOF1 is indicated above each panel. Units are arbitrary.

structure spanning much of the globe over ~ 20-50 km (similar to the trends in Figure 4c). Of greatest importance here is the time projection of the respective EOF1 patterns, which are shown in Figure 8; these illustrate the actual time development of the global anomalies projected onto the spatial EOF1 structures and effectively give globally integrated estimates of time variability. The time series in Figure 8 include both the monthly projections (smoothed with a 3-month running mean) and a low-frequency smoothed version. The $CH_4$ time series in Figure 8 are separated for variations in the lower and upper stratosphere (below 10 mb and above 6.8 mb, respectively) to isolate these regions.

The lower stratosphere $CH_4$ time series in Figure 8 shows an overall increase in time; depending on interpretation, there is either a local maximum during 1995-1996 or a decline in growth rate after 1996. This time variation is similar to that observed in tropospheric $CH_4$, where a local maximum was observed during 1991-1992 [*Dlugokencky et al.*, 1998]; this 4-year time lag between local maxima in the troposphere and stratosphere could be consistent with the "age" of air in the lower stratosphere [*Hall and Waugh*, 1997; *Waugh et al.*, 1997]. For the other three time series in Figure 8, there is a clear change in the sense of the trends before and after 1996. $CH_4$ and $H_2O$ variations in the upper stratosphere show the most dramatic changes (see Figures 3-5), with the earlier trends being reversed during 1997-1998. The slight decrease in global $H_2O$ after 1996 approximately balances the increasing $CH_4$ (in the upper stratosphere), such that the quantity $H_2O + 2CH_4$ integrated over the stratosphere is very nearly constant after 1996.

### 4.2. HF and HCl

Stratospheric HF and HCl are similar in that they both originate primarily as the photochemical breakdown products of tropospheric chlorofluorocarbons (CFCs). HF has no significant natural sources, while about 80% of stratospheric HCl originates from CFCs [*WMO*, 1989]. Trends in stratospheric HF and HCl from HALOE measurements have been studied by *Russell et al.* [1996a], who conclude that trends near the stratopause (~ 55 km) are consistent with known tropospheric CFC increases. We extend the analyses by examining structure of the trends in the latitude-height plane and the detailed time evolution through 1998.

Figure 9 shows time series of hemispheric mean anomalies in HF and HCl at 1 mb. Both constituents show monotonic increases throughout most of the HALOE record, with rapid increases prior to 1996 and a flattening of the trends during 1997-1998 (with suggestion of decreasing values of HCl in 1998). Meridional cross sections of the 1993-1997 trends in HF and HCl are displayed in Figure 10, showing statistically significant trends throughout almost the entire stratosphere. Similar overall features are seen in the HF and HCl trends in Figure 10, namely (1) an increase in the trends with altitude and (2) a relative minimum in trends in the tropics below ~ 35 km. The structure of these trends is similar to the background HF and HCl structures and also is qualitatively similar to the "age" of stratospheric air [e.g., *Hall and Waugh*, 1997; *Waugh et al.*, 1997], with largest trends corresponding to the oldest air. This is a reasonable result: since the HF and HCl trends are primarily due to the photochemical breakdown of tropospheric CFCs, air with older photochemical age will possess larger trends (and also largest absolute background amounts). There is an NH-SH asymmetry in the HF trends in Figure 10 over altitudes of ~ 30-40 km, with larger trends in the NH (also seen to a lesser degree in HCl); this is similar to the spatial structure seen in the $CH_4$ and $H_2O$ trends in Figure 4. The fact that a similar asymmetry is observed in all the long-lived trace constituents in this region suggests it is a robust signal, likely due to low-frequency variations in atmospheric transport.

EOF analysis of the global HF and HCl anomalies results in a predominant mode for each species with spatial structures that strongly resemble the trend patterns shown in Figure 10. The time variation of the EOF1 patterns are shown in Figure 11, and here the projections have only been calculated above 35 km in order to accentuate the upper stratospheric variations. The time variations for HF and HCl shown in Figure 11 reveal very linear increases through 1996, with weaker trends afterward for HF near the stratopause (consistent with the findings of *Considine et al.* [1997]). The change in HCl trends occurs about one year later than HF in Figure 11, after which a downward tendency is inferred (see also Figure 9). It is interesting that the temporal evolutions of HF and HCl in Figure 11 are qualitatively similar to those of $CH_4$ and $H_2O$ shown in Figure 8, that is, there is a decrease in the trend of each species after 1996. *Considine et al.* [1997] attribute the change in HF trend to a leveling off of

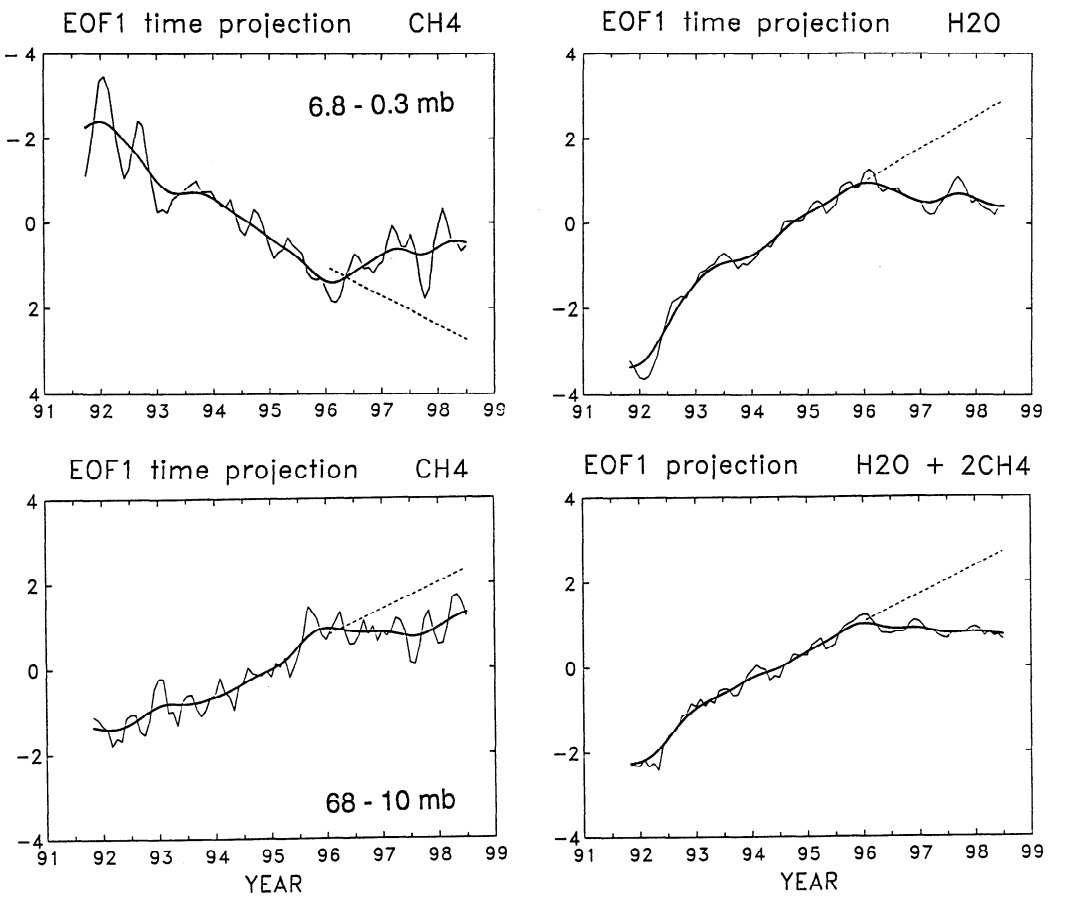


**Figure 8.** Time series of the projection of global anomalies onto EOF1 spatial structures (shown in Figure 7 for $CH_4$ and $H_2O$). Left panels show $CH_4$ projections above 6.8 mb (top) and below 10 mb (bottom). Upper right panel is the global $H_2O$ projection, and lower right panel is for $H_2O$ + $2CH_4$. The thin lines show monthly projections, while the heavy lines are temporally smoothed versions. Dashed lines show the continuation of linear trends calculated over 1993-95.

tropospheric CFCs [*Montzka et al.*, 1996], which is a reasonable assumption; however, the similarly timed changes in $CH_4$ and $H_2O$ trends suggest other dynamical or chemical processes may influence HF and HCl.

### 4.3. ClO

Chlorine monoxide (ClO) is the predominant form of reactive chlorine that destroys ozone. In the upper stratosphere (near 40 km), ClO is also the second-largest chlorine-containing species, with mixing ratios approximately 20% those of HCl. The primary source of ClO in the stratosphere is anthropogenic CFCs, with approximately 20% of the current amount due to "natural" chlorine, as discussed for HCl above. Accordingly, it is anticipated that stratospheric ClO will have increased during the UARS time frame.

The trends calculated from the MLS ClO data are rather sensitive to the time period chosen for the analysis. *Siskind et al.* [1998] present MLS ClO trends derived over 1991-1997 and 1992-1995 (from the analyses of L. Froidevaux et al., manuscript in preparation, 1998) that are a factor of 2 or more larger than the results shown here. This highlights the variable nature of trends derived from short-time records. Our results calculated over 1993-1997 are intended to be directly comparable to the other UARS trends shown here.

Calculation of ClO trends over 1993-1997 shows almost no regions of local statistical significance at particular latitudes and heights. However, global means do show significant trends. Time series of hemispheric mean ClO data at 4.6 and 2.2 mb are shown in Figure 12, showing the full variability (these time series have not been deseasonalized or had QBO effects removed). Data at 4.6 mb show a statistically significant trend of 0.015 ± 0.010 ($2\sigma$ uncertainty) ppmv per year, and this is the only altitude where the 1993-1997 trend is significant. The time series at 2.2 mb in Figure 12 shows a series of low values during 1992, so that it is evident the trends over 1992-1995 [*Siskind et al.*, 1998] will be much larger than those over 1993-1997.

The vertical profiles of time mean ClO and HCl are shown in Figure 13, based on MLS and HALOE data averaged over 60°N-S. Also shown here are vertical profiles of the global trends expressed in mixing ratio (ppbv/year) and trends calculated as percentage values. The global HCl trends are significant at all altitudes, whereas ClO trends are only significant at 4.6 mb. The mixing ratio trends in ClO and HCl in the upper stratosphere (near 35-45 km) are similar in proportion to the background values so that the percentage trends are about the same (~ 2-3% per year). Because ClO and HCl trends in the upper stratosphere are both tied to tropospheric CFC increases, the approximately constant percentage increases in both constituents provides a consistency check on each individual species. Furthermore, since

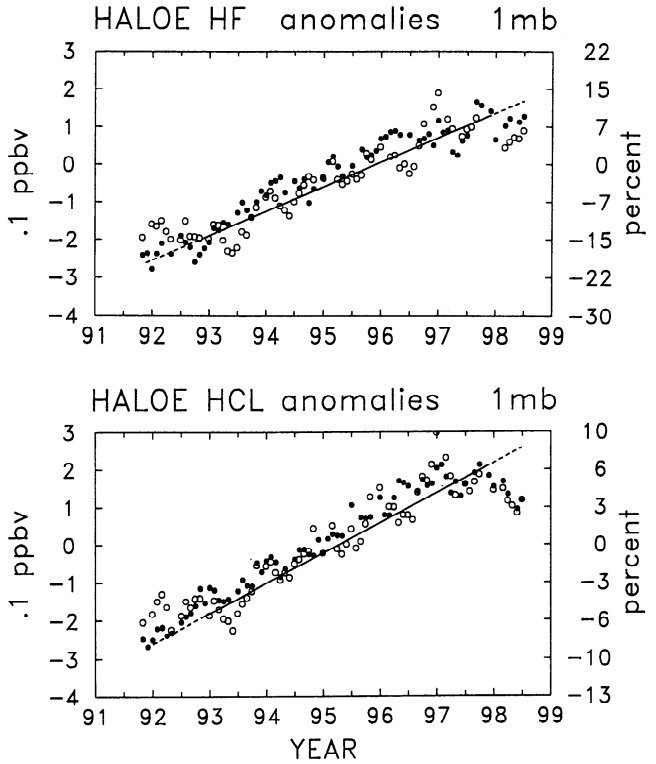


**Figure 9.** Time series of hemispheric (top) HF and (bottom) HCl anomalies at 1 mb for NH (solid circles) and SH (open circles) data, along with the 1993-1997 trends.

*Russell et al.* [1996a] have demonstrated that the stratospheric HCl trends are consistent with tropospheric CFC trends, the results in Figure 13 suggest that this consistency extends to stratospheric ClO trends also.

### 4.4. Ozone

The HALOE and MLS data provide two independent measurements of ozone trends over the UARS lifetime. These data complement each other in terms of measurement technique (solar occultation versus microwave emission) and space-time sampling. Figure 14 shows meridional cross sections of trends in ozone from HALOE and MLS over 1993-1997 plotted in units of percent per year (with respect to local background values); note the greater altitude range and higher vertical resolution available with the HALOE results. The HALOE trends show significant negative trends near 30-35 km (near the mixing ratio maximum) over 30°N-S with maximum values of ~ -1% per year. Significant positive trends are observed below this region (with maximum at the 32-mb level) centered near the equator (~ 10°N-S). Negative trends of order –0.5% per year are also seen in the HALOE data over middle to high latitudes in the upper stratosphere, but these are not significant.

The MLS trends show significant negative trends in the tropical middle stratosphere (over 30-40 km) reasonably similar in spatial structure and magnitude (~ -1% per year) to the HALOE trends but extending to higher altitudes. MLS also shows positive trends at lower altitudes in the tropics in reasonable agreement with HALOE. Note that there is a difference in vertical sampling between the HALOE and MLS data (data levels are indicated on the right-hand axes in Figure 14), and this may influence differences in detail for trends in these data.

Figure 15 shows trends derived from SAGE II ozone data for the same period (1993-1997) as the HALOE and MLS calculations in Figure 14. The SAGE II trends look reasonably similar overall to the HALOE and MLS results. The most distinctive feature in the SAGE II data is the positive tropical trends near 25 km, as seen also in the HALOE and MLS data. The negative tropical trends near 30-35 km observed in HALOE and MLS data are weaker and not significant in the SAGE II results (except near 20°N).

Figure 16 compares time series of the tropical ozone anomalies from HALOE, MLS, and SAGE II (the latter spanning late 1984-1997) for the 10- and 32-mb levels (interpolated from the 46- and 22-mb levels for MLS data). All three data sets show reasonable agreement for low-frequency variations at 32 mb during 1992-1997. Comparison with the longer record of SAGE II data (back to 1984) suggests there was a substantial drop in ozone at 32 mb following the eruption of Mt. Pinatubo in 1991 followed by a slow return to prevolcanic ozone levels by approximately 1996. The time series at 10 mb in Figure 16

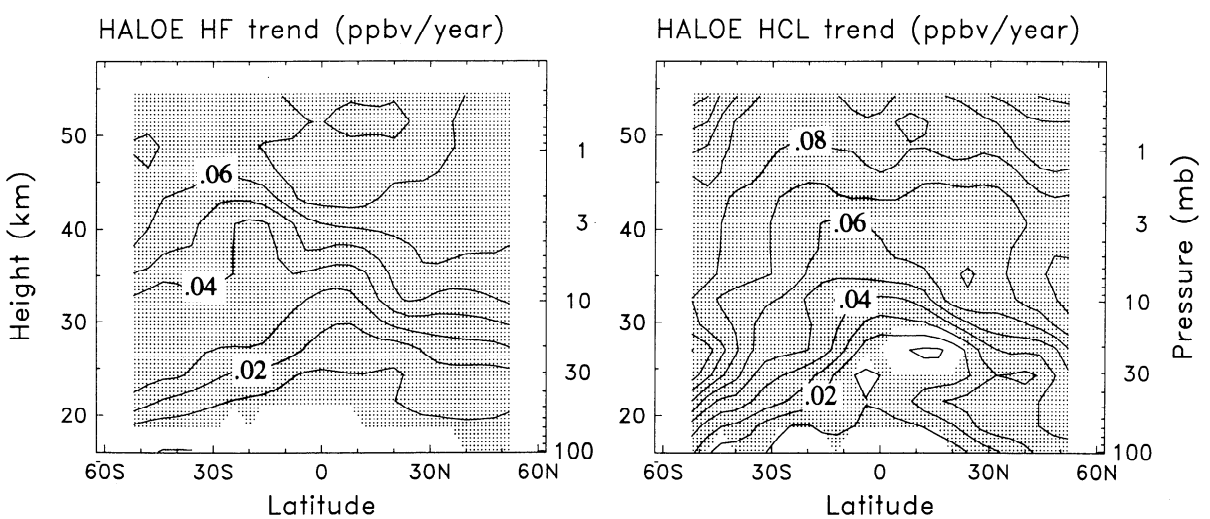


**Figure 10.** Meridional cross sections of trends in (left) HF and (right) HCl. Units are ppbv per year in both panels, and shading denotes 95% statistical significance.

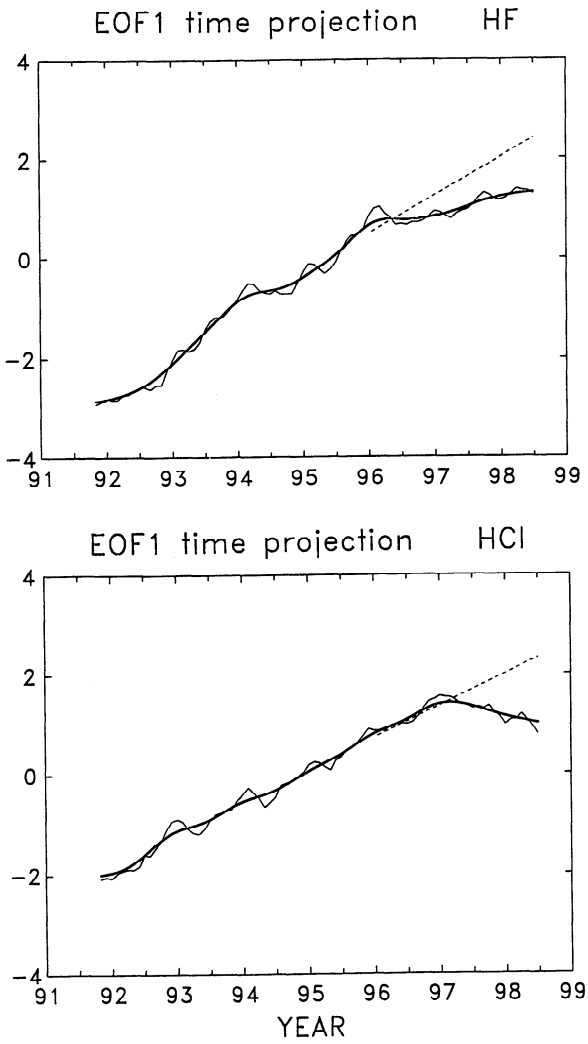


**Figure 11.** Time series of the projection of EOF1 for (top) HF and (bottom) HCl calculated over 35-55 km. The spatial patterns of the respective EOFs are not shown, but are similar to the trends in Figure 10.

shows clear negative trends in HALOE and MLS data, but such a trend is less evident in the SAGE II measurements.

Overall, the HALOE, MLS, and SAGE II ozone trends over 1993-1997 show reasonably similar spatial structures (Figures 14 and 15). However, these short-term ozone variations are very different from trends derived from longer time records of SAGE I and II data (1979-1996) or SAGE II data alone (1984-1996) [*SPARC*, 1998]. These decadal-scale SAGE trends highlight significant ozone decreases in the upper stratosphere (maximum near 40-45 km) outside of the tropics, with magnitude of order –0.6% to –0.8% per year. Similar trends are also found in Umkehr and Solar Backscatter Ultraviolet (SBUV/(2)) data by *SPARC* [1998]. Negative trends of this magnitude are seen in the high-latitude upper stratosphere in the shorter-term HALOE, MLS, and SAGE II records (Figures 14 and 15), but there is not strong spatial coherence or statistical significance. More importantly, the strongest trend signals seen in Figures 14 and 15 of tropical ozone loss near 30-35 km and increases below are not found in the longer SAGE records. The 32-mb SAGE II time series seen in Figure 16 suggests large and long-lasting effects on tropical ozone related to the Mt. Pinatubo eruption in 1991, and this is one obvious mechanism for trends over 1993-1997 being very different from longer records (back to 1979). These demonstrated differences in ozone trends caution that the changes observed in other constituents during the UARS lifetime are not necessarily representative of decadal time scales.

### 4.5. $NO_2$

Nitrogen dioxide ($NO_2$) is an important component of the reactive nitrogen budget in the stratosphere. $NO_2$ has a strong diurnal variation, and HALOE provides independent sunrise and sunset measurements, which are analyzed separately here. The mean values of $NO_2$ peak in the middle stratosphere (~ 35 km), with sunset values approximately twice as large as those at sunrise [*Nevison et al.*, 1996].

Meridional cross sections of the trends in HALOE sunrise and sunset $NO_2$ data are shown in Figure 17, and vertical profiles of the trends over 30°N-S are shown in Figure 18. Both sunrise and sunset observations show significant positive trends with maxima in the tropics over 25-35 km (slightly below the mixing ratio peaks; see Figure 18). Statistical significance for the 30°N-S trends extends over 20-40 km (Figure 18). The sunset trends (measured in mixing ratio) are approximately twice as large as those at sunrise, such that the percentage increases (also shown in Figure 18) are similar at sunrise and sunset (~ 3-4% per year near 30 km and larger values below). Time series of sunset $NO_2$

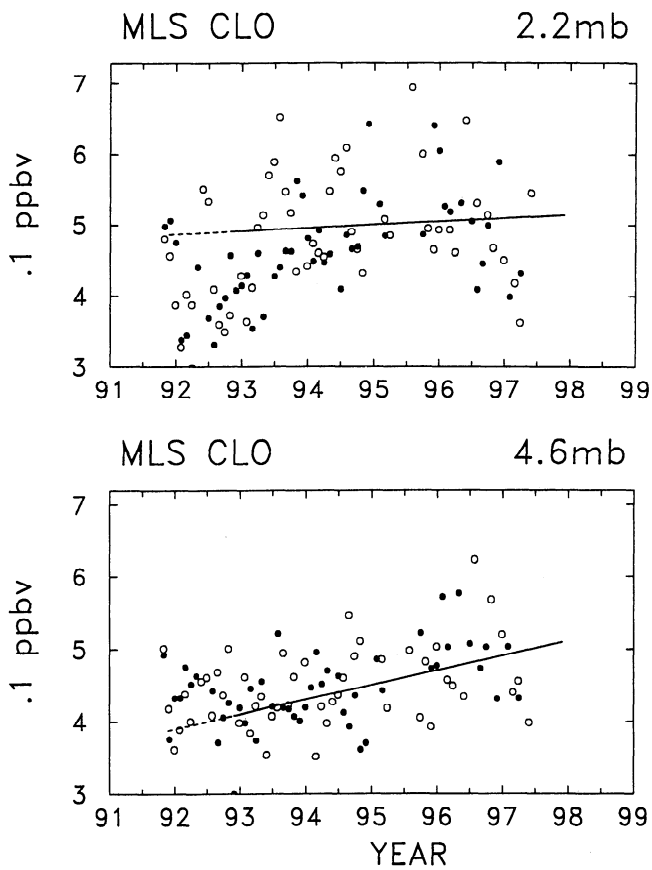


**Figure 12.** Time series of hemispheric mean ClO data at (top) 2.2 mb and (bottom) 4.6 mb. Solid and open circles denote NH and SH data, respectively. These time series have not been deseasonalized, but show the full variability. Lines show the global trend fits over 1993-1997.

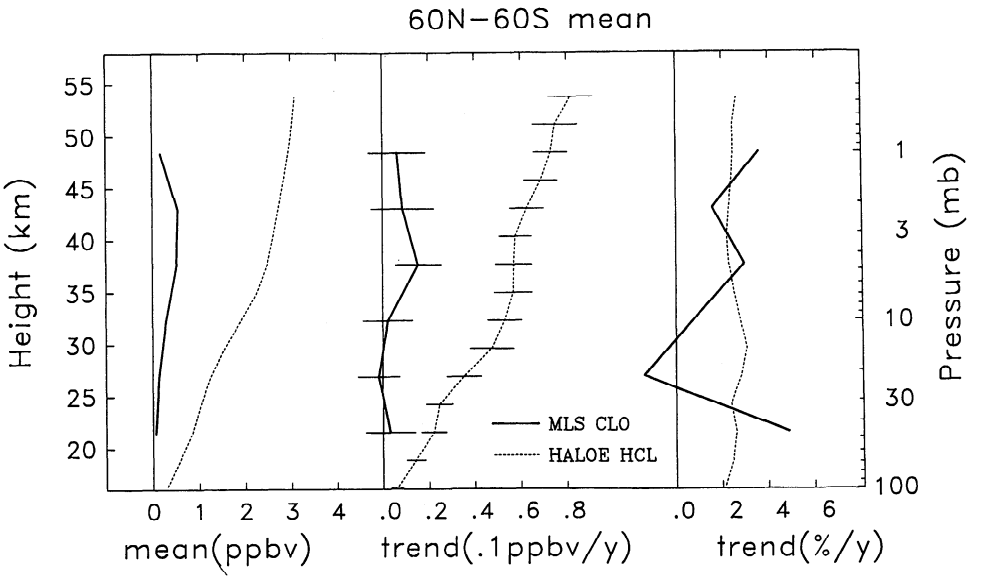


**Figure 13.** (left) Vertical profiles of ClO and HCl time mean background structures and (middle and right) trends for data averaged over 60°N-S. Trends are shown in both mixing ratio (middle) and percentage (right) values. The error bars on the middle curves indicate 2 σ uncertainties.

anomalies at 14.6 mb (~ 30 km) averaged over 30°N-S are shown in Figure 19, showing a clear upward trend over 1993-1997.

The spatial maximum in $NO_2$ trends (Figure 17) approximately overlaps the region of strongest negative ozone trends in the tropical middle stratosphere (near 30 km; see Figure 14). In this altitude region, ozone catalytic destruction is dominated by $NO_x$ [e.g., *Osterman et al.*, 1997], so a strong anticorrelation between ozone and $NO_2$ is expected. The space-time character of this anticorrelation is explored further by a singular value decomposition (SVD) analysis [see *Wallace et al.*, 1992]; this is analogous to an EOF analysis for one variable, but searches for optimal modes of covariance between two fields ($O_3$ and sunset $NO_2$ anomalies in this instance). The results (shown in Figure 20) show spatially correlated maxima in the tropical middle stratosphere with $O_3$ and $NO_2$ out of phase near 30 km (and a secondary ozone maximum centered near 24 km in phase with $NO_2$); these patterns are similar to the linear trends in Figures 14-17. The time projections of the $O_3$ and $NO_2$ anomalies in Figure 20 show substantial high-frequency variability; however, the temporally smoothed time series suggest a change in the slope in the latter part of the record (with strongest trends prior to 1996). These time variations are qualitatively similar to those observed for $CH_4$, $H_2O$, HF, and HCl above (Figures 8-11).

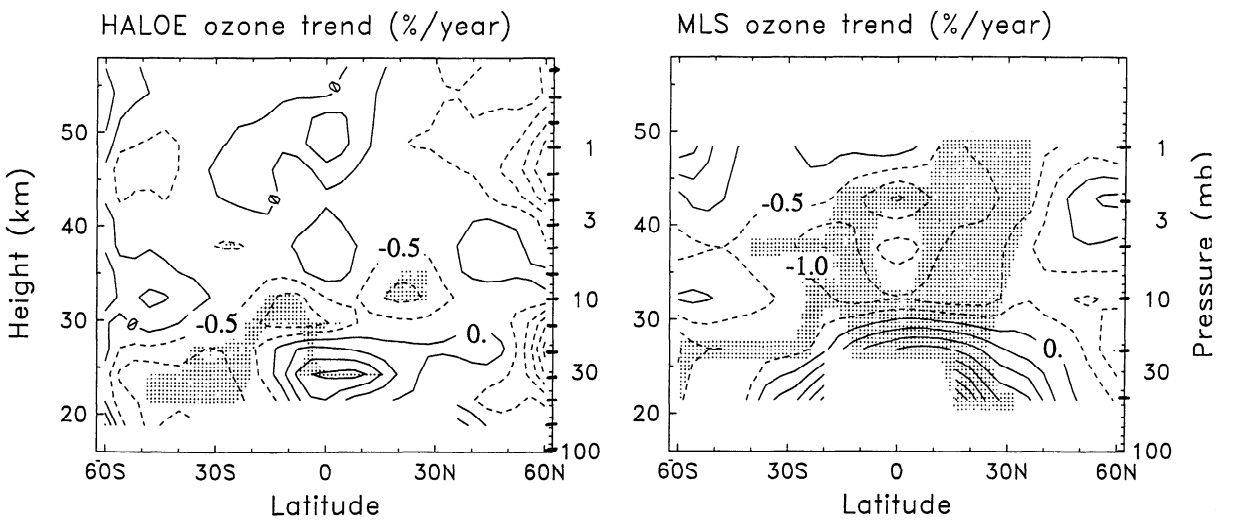


**Figure 14.** Meridional cross sections of ozone trends during 1993-1997 calculated from (left) HALOE and (right) MLS data. Values are shown in local percent per year (relative to the long-term means), and shading denotes statistical significance. Trends are only shown over regions where the background ozone is greater than 1 ppmv. Tick marks on the right axes denote data levels; note the MLS data only cover 46-1 mb and have half the vertical resolution of the HALOE data.

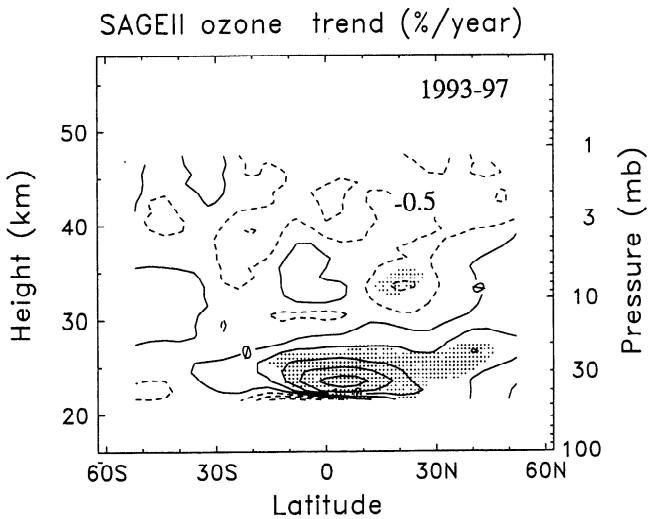


**Figure 15.** Ozone trends during 1993-1997 calculated from SAGE II data. Contour interval is 0.5 % per year, and shading denotes statistical significance.

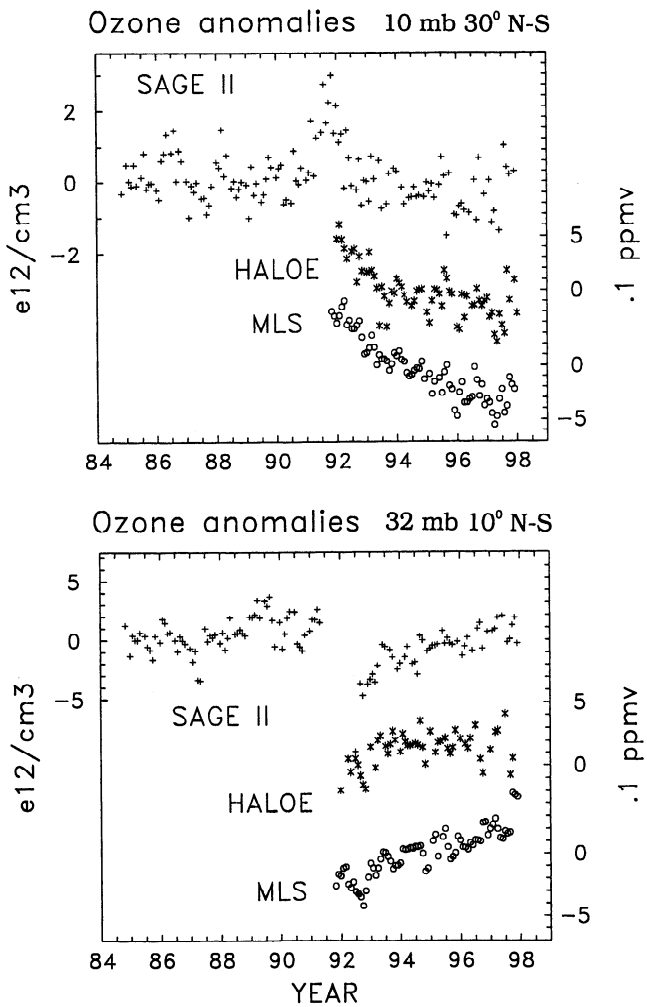


**Figure 16.** Time series of tropical ozone anomalies from SAGE II, HALOE and MLS data. (top) Data at 10 mb over 30°N-S and (bottom) at 32 mb over 10°N-S. The SAGE II data are expressed in terms of ozone density (left axes) and HALOE and MLS in terms of mixing ratio (right axes). The time series are offset for clarity.

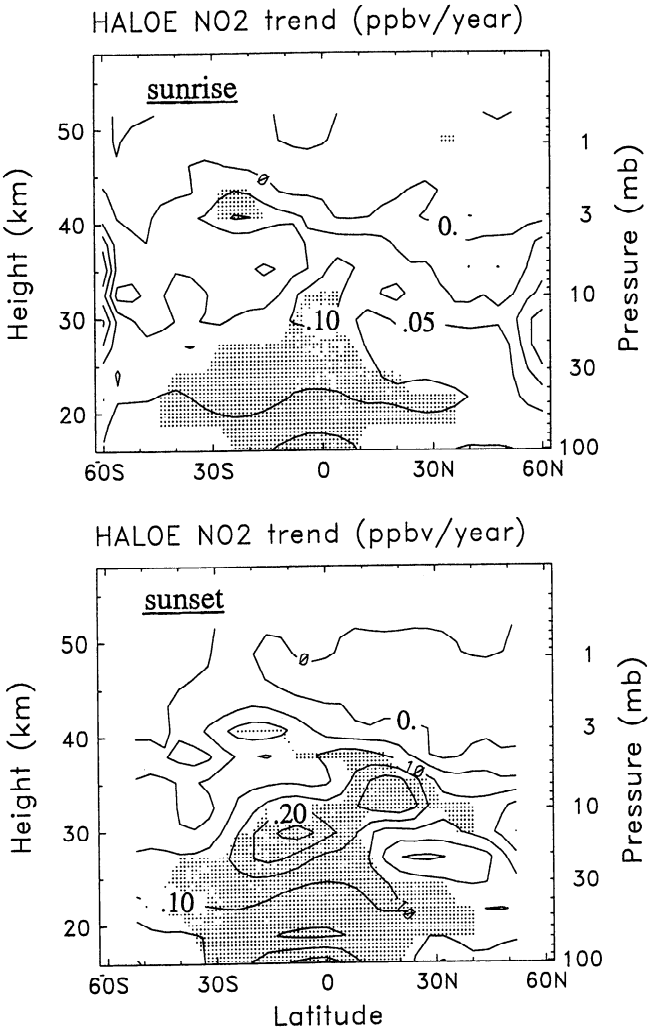


**Figure 17.** Meridional cross sections of trends in HALOE $NO_2$ data for measurements made at (top) sunrise and (bottom) sunset. Contour interval in both panels is 0.05 ppbv per year, and shading denotes statistically significant trends.

### 4.6. $HNO_3$

Nitric acid ($HNO_3$) also contributes a substantial fraction of the stratospheric odd nitrogen budget; it is the dominant component in the lower stratosphere. Figure 21 shows trends in the MLS $HNO_3$ data during 1993-1997 (recall that these data are only retrieved on pressure levels of 100, 46, and 22 mb). Significant negative trends are observed in $HNO_3$ in both hemispheres outside of the tropics with somewhat larger trends in the NH. The trends of order –0.2 ppbv per year in Figure 21 correspond to percentage variations of ~ -2% per year over these five years. Figure 22 shows time series of $HNO_3$ hemispheric mean anomalies at 46 mb, illustrating the downward trend in both hemispheres. There are also relatively high $HNO_3$ anomalies in both hemispheres during 1992, probably due to the influence of Mt. Pinatubo aerosols [see *Koike et al.*, 1994; *David et al.*, 1994; *Coffey*, 1996]. Figure 23 shows time series of aerosol surface area (which is proportional to the heterogeneous chemical reaction probability) in the lower stratosphere derived from SAGE II measurements (*Thomason et al.* [1997], updated through 1997). These data quantify the very large aerosol surface area in 1992 (due to Pinatubo), corresponding to the high $HNO_3$

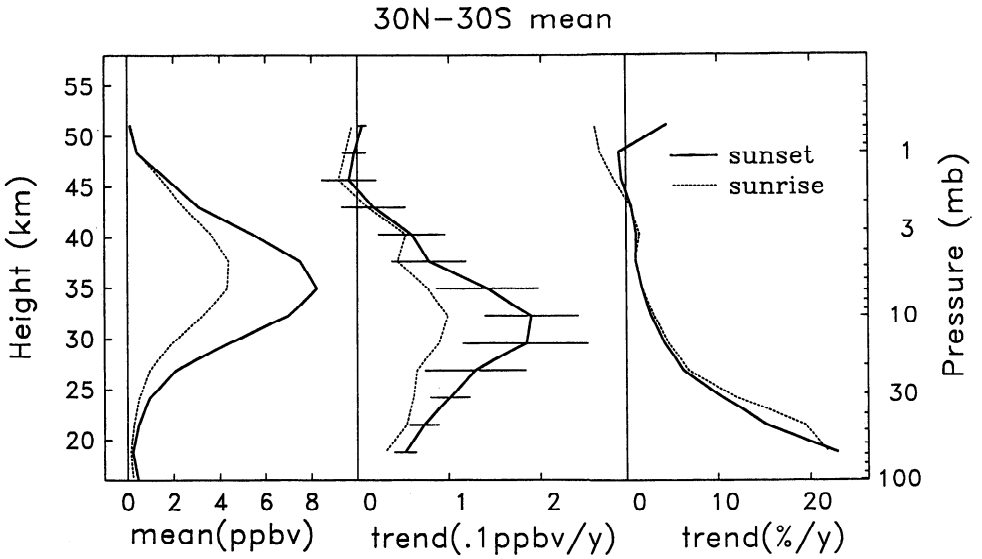


**Figure 18.** Vertical profiles of HALOE sunrise and sunset $NO_2$ (left) time means and (middle and right) trends for data averaged over 30°N-S. Trends are shown in both mixing ratio (middle) and percentage (right) values. Error bars on the sunset trends in the middle panel denote 2 σ uncertainties.

anomalies in Figure 22. For later discussion, note the aerosol surface area returns to relatively small values by late 1994, with small changes since that time (although the amount of aerosol continues to slowly decline).

The main source of $HNO_3$ in the stratosphere is $NO_2 + OH \rightarrow HNO_3$, and $NO_2$ is also a product of $HNO_3$ photolysis ($HNO_3 + h\nu \rightarrow OH + NO_2$). Because of this coupling, it is interesting to compare the absolute amount of increase in $NO_2$ observed by HALOE with the observed decrease in $HNO_3$ measured by MLS. To that end, we calculate the global mean column integrals of the anomalies in each species according to

$$\langle \chi \rangle = \left( \frac{N_A}{W} \right) \frac{\Sigma dz \Sigma \cos\phi d\phi [\rho(z)\chi'(\phi,z)]}{\Sigma \cos\phi d\phi} \qquad (1)$$

Here $\rho(z)$ is the background atmospheric density ($\rho = \rho_0 \exp(-z/7$ km)), $\chi'(\phi,z)$ is the constituent anomaly, $N_A$ is Avogadro's number, and $W$ is the respective molecular weight for $NO_2$ (46) or $HNO_3$ (63). Vertical integrals are calculated over 100-4.6 mb for sunset $NO_2$ (the region of largest trends in Figure 17) and 100-22 mb for $HNO_3$. The objective is to compare as directly as possible changes in the total stratospheric burdens of $NO_2$ and $HNO_3$. Time series of these global column anomalies are shown in Figure 24, showing that the absolute amount of $HNO_3$ decrease over 1993-1997 is about a factor of 2 larger than the $NO_2$ increase: the corresponding 1993-1997 trends are − 0.20 ± 0.04 for $HNO_3$ and + 0.12 ± 0.02 for $NO_2$ (with units of $10^{14}$/cm$^2$ per year). The larger absolute $HNO_3$ trends are principally the result of their occurring in the lower stratosphere; there is approximately a factor of 5 density variation between the $HNO_3$ maxima in Figure 21 and the $NO_2$ maxima in Figure 17. These results suggest that there is a partial cancellation in the changing amounts of $NO_2$ and $HNO_3$ in the stratosphere during 1993-1997, similar to compensating changes observed after Mt. Pinatubo [*Koike et al.*, 1994; *Coffey*, 1996]. However, the $HNO_3$ column trends are still about a factor of 2 larger than those in $NO_2$. This difference could be due to several reasons, such as (1) positive $HNO_3$ trends outside the region sampled by MLS, such that the column $HNO_3$ and $NO_2$ trends more nearly balance; (2) unknown instrument trend uncertainties; or (3) an additional mechanism for depleting $HNO_3$ in the lower stratosphere.

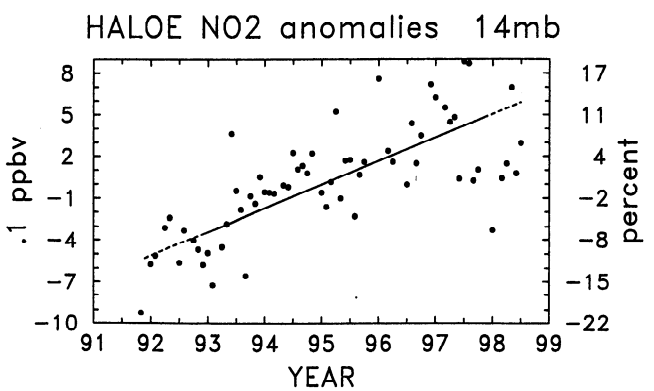


**Figure 19.** Time series of $NO_2$ sunset anomalies at 14 mb for data averaged over 30°N-S.

## 5. Summary and Discussion

The relatively long record of stratospheric constituent observations from UARS shows evidence of monotonic changes (trends) in every constituent over at least some regions of the stratosphere. In fact, the trend component is usually apparent to the eye in time series of anomalies (especially if the seasonal cycle and QBO variations are removed previously). Our objective here has been to describe the space-time characteristics of these trends in all the constituents observed by the HALOE and MLS instruments and to search for coherent behavior among the different species. The most important results are summarized and discussed here.

Methane ($CH_4$) increased in the lower stratosphere during 1993-1997 at a rate of 0.86 ± 0.40% per year, consistent with observed tropospheric increases (prior to 1992). $CH_4$ decreased in the upper stratosphere at a rate of ~ -4 ± 1.5% per year during 1993-1997, but recent data for 1997-1998 show a reversal of

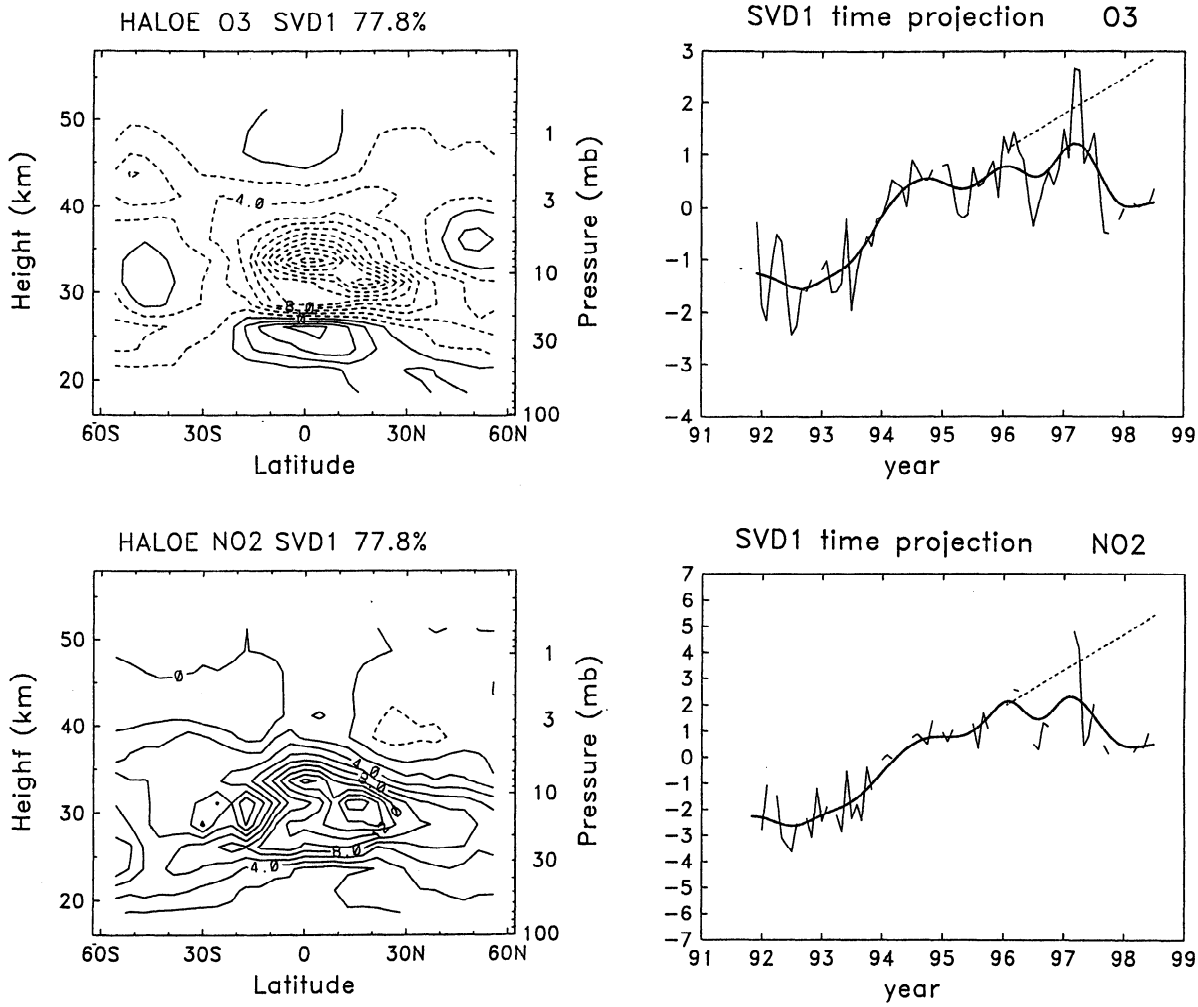


**Figure 20**. (left) Spatial patterns and (right) time projections for the leading mode of covariance between HALOE ozone and sunset $NO_2$ residuals. Ozone structure is on top and $NO_2$ on bottom. The dashed lines in the right-hand panels show the continuation of linear trends calculated over 1993-1995.

these earlier trends. The mechanism for the upper stratospheric decrease for the earlier period is not well understood. One possible contribution is increasing chemical destruction due to chlorine chemistry [see *Lary and Toumi,* 1997], although idealized model results suggests this may only account for ~ -1 to –2% per year (C. Granier, personal communication, 1997). *Nedoluha et al.* [1998b] have suggested a large perturbation in stratospheric circulation may also have contributed to this decrease, and the transient nature of the observed trends is consistent with such an impulsive forcing. One obvious mechanism for such a change is the Mt. Pinatubo volcanic eruption in June 1991. Idealized model studies [e.g., *Brasseur and Granier*, 1992; *Rosenfield et al.*, 1997] have suggested an increase in tropical vertical velocity by 10-20% following the eruption, and more detailed aerosol heating calculations by *Eluszkiewicz et al.* [1997] suggest possibly larger perturbations. However, these calculations all suggest that the Pinatubo circulation anomaly decayed to small values by the end of 1992, whereas the upper stratospheric $CH_4$ anomalies (Figure 3) show monotonic decreases until approximately 1996.

HALOE data show increases in water vapor throughout most of the stratosphere at a rate of ~ 1.5% per year during 1993-1997. These trends appear to flatten or change sign (in the upper stratosphere) after 1996, similar to the $CH_4$ time series. The magnitude of $H_2O$ increase during 1993-1997 is much larger than can be accounted for by methane oxidation (Figure 6; see also *Nedoluha et al.* [1998a]). The variable component of stratospheric total hydrogen ($H_2O$ + $2CH_4$) shows significant increases (~ 1% per year) prior to 1996, but more constant values after 1996. The trends prior to 1997 suggest some mechanism for increased $H_2O$ transport into the stratosphere. The main mechanism for water vapor transport into the stratosphere is via the mean upward circulation in the tropics [e.g., *Mote et al.*, 1996], although the details of where and when the transport occurs are poorly understood at present. *Nedoluha et al.* [1998a] have suggested that a temperature increase of ~ 0.1 K per year near the tropical tropopause could account for the observed stratosphere $H_2O$ trends, and small changes in tropopause pressure could also influence short-term trends. Although there is not evidence for warming trends in the tropical lower stratosphere from long-term radiosonde or satellite data [*WMO*, 1998], there is less detailed information available at present on variability of the global tropical tropopause.

Two new pieces of information regarding $CH_4$ and $H_2O$ trends arise from this study. First, there are clear spatial structures in the $CH_4$ and $H_2O$ trends in the middle stratosphere (Figure 4)

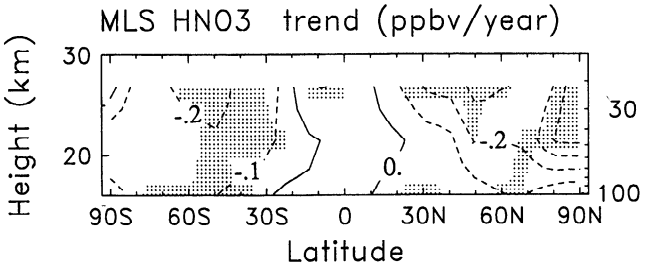


**Figure 21.** Meridional cross section of linear trends in MLS $HNO_3$ data. Contour interval is 0.1 ppbv per year, and shading denotes statistically significant trends. Note data are only available over 100-22 mb.

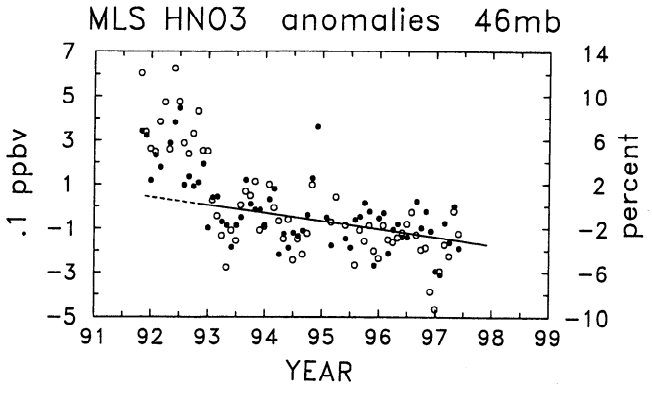


**Figure 22.** Time series of hemispheric anomalies in $HNO_3$ data at 46 mb, for NH (solid) and SH (open circles) data. Straight line is the 1993-1997 trend fit.

with an asymmetry between the hemispheres. These patterns are mirrored in both $CH_4$ and $H_2O$, such that they cancel in the quantity $H_2O + 2CH_4$ (Figure 4). Because the conversion of $CH_4$ into $H_2O$ depends on the residence time in the stratosphere, these spatial patterns are evidence of low-frequency variations in atmospheric transport in the middle stratosphere (such that the air is somewhat older in the Northern Hemisphere (NH) and younger in the Southern Hemisphere (SH) over 30-40 km). Similar spatial structures (and implications) are derived from the HF trends (Figure 10).

A second important point is that time variations in the trends of $H_2O$ and $CH_4$ reveal an apparent discontinuity near the beginning of 1996 (Figure 8) with substantially weaker (or reversed) trends after this time. A qualitatively similar time variation is observed in the HF and HCl time series (Figure 11) and is also suggested in $O_3$ and $NO_2$ data (Figure 20).

The appearance of a similar changing trend in many constituents is suggestive of some true atmospheric change, although only speculation on the mechanism(s) can be offered. The evidence for changing trends in several long-lived constituents argues for some corresponding change in the large-scale stratospheric circulation. An impulsive response to the Mt. Pinatubo eruption in June 1991 is one obvious impact to the stratospheric system, but model calculations [e.g., *Rosenfield et al.*, 1997] and stratospheric temperature observations [*Randel et al.*, 1995; *Angell*, 1997] suggest that much of the Pinatubo impact decayed to background values within 1-2 years. One possibility is that the impulsive Pinatubo change could produce radiative-chemical couplings which somehow extend global effects until 1996. One mechanism for such coupling could be ozone in the tropical lower stratosphere, which shows substantial changes after Pinatubo, and a response time of order 4 years to return to prevolcanic equilibrium (Figure 16). Because ozone radiative effects influence tropical upwelling, the observed ozone changes could modulate stratospheric circulation on this same timescale. Another possible contributor is solar variability:

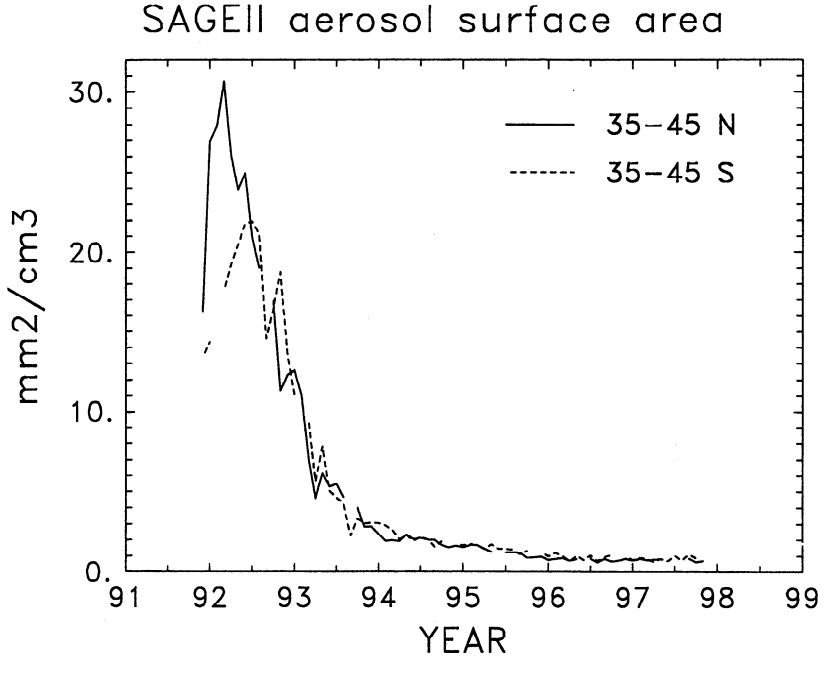


**Figure 23.** Time series of aerosol surface area at 20.5 km in the NH and SH midlatitudes (35°-45°N-S) derived from SAGE II measurements. These data are an update of the time series shown by *Thomason et al.* [1997, Figure 1].

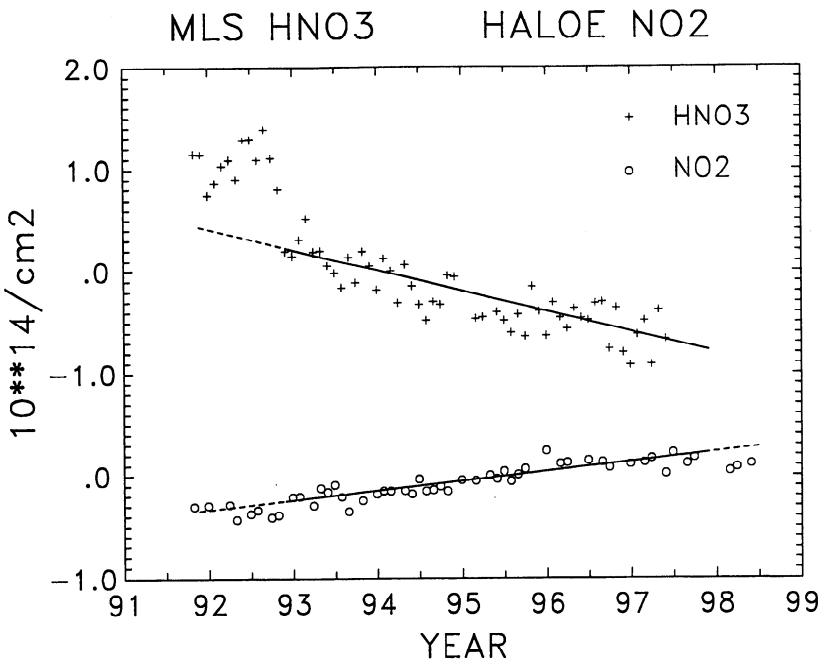


**Figure 24.** Time series of global column integrals (equation 1) for anomalies in MLS $HNO_3$ and HALOE sunset $NO_2$. Straight lines are the 1993-1997 trend fits.

although the solar cycle is at a relative minimum during 1993-1997 careful inspection of Figure 2 shows a decline in implied solar forcing during 1993-1995 with a flattening in early 1996 (similar to the constituent variations) and an increase in 1998. However, large stratospheric circulation changes are not anticipated from these relatively small solar variations, so we do not expect this to be an important effect.

The spatial structure of HF and HCl trends (Figure 10) are both similar to patterns of their respective time mean backgrounds, with maxima in the upper stratosphere and minima in the tropical lower-middle stratosphere. This is reasonable, as the presence of these constituents in the stratosphere is in fact due to trend-like growth (related to tropospheric CFCs). The trends maximize in the upper stratosphere because that is where the photochemical CFC breakdown is maximum [see *Russell et al.*, 1996a]. These trend (and background) patterns are both similar to patterns of the "age" of stratospheric air [e.g., *Hall and Waugh*, 1997; *Waugh et al.*, 1997] with smaller values in the tropics reflecting the upwelling of relatively young, less photochemically aged air. The HF trends, and to a lesser degree those for HCl, show both the NH-SH asymmetries over 30-40 km, and a decrease in the trend rates after 1996, observed in the $H_2O$ and $CH_4$ trends. *Considine et al.* [1997] have attributed the decreasing HF trends near the stratopause to the observed decrease in tropospheric CFCs [*Montzka et al.*, 1996] with a time lag of ~ 4 years. Although this is a reasonable conclusion, the observation of similar temporal behavior for the long-lived constituents of $H_2O$ and $CH_4$ (whose sources are presumably independent of tropospheric CFCs), and for $O_3$ and $NO_2$, suggests there may be variations in transport or chemistry additionally affecting the HF and HCl trends.

The MLS ClO data show significant positive trends in the upper stratosphere for large area means. The magnitude of the calculated ClO trends varies substantially depending on the time period chosen: the results shown here (over 1993-1997) are substantially smaller than those shown by *Siskind et al.* [1998] for the periods 1992-1995 and 1991-1997. Our 1993-1997 ClO trends show a percentage rate of increase that is very similar to that observed for HCl during the same time period (~ 2-3% per year). This is a reasonable result, assuming that both the ClO and HCl trends originate from tropospheric CFCs [e.g., *Russell et al.*, 1996a], although *Siskind et al.* [1998] argue that differences in the HCl and ClO trend rates might be expected because of decreasing $CH_4$ in the upper stratosphere. Although the global mean ClO trends are significant at the 4.6 mb level, there is little information that can be derived from the spatial structure of the ClO trends; there is a large degree of variability (either atmospheric or instrumental) and little statistical significance for local ClO trends.

Ozone trends calculated from the HALOE and MLS data over 1993-1997 show reasonably similar results (Figure 14) with negative trends of order ~ -1% per year in the tropical middle stratosphere, and increases in the lower stratosphere (near 25 km) of 1-2% per year. Direct comparison with SAGE II trends over 1993-97 shows reasonable agreement, particularly in the tropical lower stratosphere, and the similar findings from three independent measurement systems gives confidence in these results. Comparison with the longer record of SAGE II data (back to 1984) suggests that the lower stratospheric ozone trends over 1993-1997 are strongly influenced by a prolonged recovery to Mt. Pinatubo in 1991: the time series at 32 mb (Figure 16) suggests the prevolcanic equilibrium is not reached until ~ 1996. This is probably the main reason why the ozone trends over 1993-1997 are fundamentally different in character to the longer-term trends (~1979-1996) presented in the recent assessments by *SPARC* [1998] and *WMO* [1998]. These clear differences caution against interpretation of other constituent trends from UARS as representative of longer-term (decadal) trends.

The mechanism(s) for the extended effects of Mt. Pinatubo on tropical ozone near 25 km are not known. The ozone equilibrium in this region is primarily a balance between photochemical production and upward transport [e.g., *Avallone and Prather*, 1996] such that increased circulation corresponds to relatively low ozone. The slow return to prevolcanic equilibrium may be

evidence for Pinatubo circulation effects beyond the 1-2 year timescale derived in model or diagnostic calculations [*Rosenfield et al.*, 1997; *Eluszkiewicz et al.*, 1997]. Other possibilities include a self-healing effect associated with observed tropical ozone loss above 28 km (a decrease in upper level ozone allowing penetration of more ultraviolet light, leading to enhanced ozone production) or photochemical ozone loss associated with Pinatubo aerosols.

The observed ozone decrease in the tropical middle stratosphere over ~ 28-35 km is likely associated with spatially coherent increases in $NO_2$ observed in this region. Both sunrise and sunset $NO_2$ observations from HALOE show statistically significant increases over ~ 20-40 km. The trends in mixing ratio maximize near 30-32 km, slightly below the peak in background $NO_2$ (which is near 35 km). The spatial out-of-phase coincidence between trends in $O_3$ and $NO_2$ (in the tropics over 28-35 km) is physically consistent with the dominant control of $NO_x$ catalytic cycles for ozone destruction in this region [see, e.g., *Osterman et al.*, 1997]. The mechanism(s) behind the observed $NO_2$ increases are not known; *Nedoluha et al.* [1998b] suggest a combination of transport and solar cycle effects (although there are relatively small solar variations during 1993-1997). The percentage increases in $NO_2$ vary from ~ 2 to 10% per year over 25-35 km (decreasing with altitude; see Figure 18); these values are much larger than the ~ 0.3% per year increase observed in tropospheric $N_2O$ [*WMO*, 1998], so the stratospheric increase is not simply following the troposphere. An intriguing piece of the puzzle is that the coherent $O_3$- $NO_2$ variations exhibit an apparent flattening of the trend after 1996 (Figure 20), similar to the time variations seen in other constituents here.

The MLS $HNO_3$ data show strong changes over the 1991-1997 record. The time series show a rapid increase from 1991 to early 1992, followed by a relatively strong decrease during late 1992, and this is similar to changes observed in ground-based column $HNO_3$ measurements [*Koike et al.*, 1994], which are attributable to Pinatubo aerosols (see *Coffey* [1996], and the aerosol record in Figure 23). After 1993 the MLS $HNO_3$ data show a continued decline in both hemispheres at a rate of ~ -2% per year (during 1993-1997). Time series of aerosol measurements in the lower stratosphere from SAGE II data (Figure 23) indicate the majority of aerosol surface area changes (the important quantity for heterogeneous chemistry variations) occurred by the end of 1994, although levels continue to decrease slowly through the present time. It is difficult to interpret detailed time variations in the global $HNO_3$ data after 1993; the 46 mb data (Figure 22) suggest a possible flattening of the $HNO_3$ trends after 1994 similar to the SAGE II aerosol surface area, but this is less evident in the global column integrals (Figure 24). We note the model results of *Rosenfield et al.* [1997] also suggest the direct heterogeneous chemical effects on $HNO_3$ from Pinatubo were not large after 1994.

Because $HNO_3$ and $NO_2$ are coupled chemically in the stratosphere, it is interesting to compare changes in globally integrated column amounts. We find that the decreases in column $HNO_3$ are about a factor of 2 larger than column increases in sunset $NO_2$ data from HALOE. This suggests either unresolved trends in $HNO_3$ outside the region of MLS data, instrumental uncertainties, or another mechanism for removing $HNO_3$ in the lower stratosphere.

In summary, the UARS data show trends in $CH_4$ (in the upper stratosphere), $H_2O$, $O_3$, $NO_2$, and $HNO_3$ that are not well understood. Additionally, the changing trend rates after 1996 is an intriguing and poorly understood aspect of these data. Hopefully, the continued operation of UARS will allow the details of these trends to be tracked well into the future.

**Acknowledgments.** We thank Claire Granier, Susan Solomon, and Bill Mankin for discussions throughout the course of this work, and Lucien Froidevaux, Rolando Garcia, Michelle Santee, and Anne Smith for comments on the paper. We thank Larry Thomason for providing updated SAGE II aerosol measurements for the generation of Figure 23 and Joe Zawodny for 1997 SAGE II ozone data. Marilena Stone expertly prepared the manuscript. This work was partially sponsored under NASA grants W-18181 and W-16215. NCAR is sponsored by the National Science Foundation.

## References

Angell, J. K., Stratospheric warming due to Agung, El Chichon, and Pinatubo taking into account the quasi-biennial oscillation, *J. Geophys. Res., 102*, 9479-9485, 1997.

Avallone, L. M., and M. J. Prather, Photochemical evolution of ozone in the lower tropical stratosphere, *J. Geophys. Res., 101*, 1457-1461, 1996.

Barath, F., et al., The Upper Atmosphere Research Satellite Microwave Limb Sounder Instrument, *J. Geophys. Res., 98*, 10,751-10,762, 1993.

Brasseur, G., and C. Granier, Mount Pinatubo aerosols, chlorofluorocarbons, and ozone depletion, *Science, 257*, 1239-1242, 1992.

Brühl, C., et al., Halogen Occultation Experiment ozone channel validation, *J. Geophys. Res., 101*, 10,217-10,240, 1996.

Coffey, M. T., Observations of the impact of volcanic activity on stratospheric chemistry, *J. Geophys. Res., 101*, 6767-6780, 1996.

Considine, G. D., L. Deaver, E. E. Remsberg, and J. M. Russell III, HALOE observations of a slowdown in the rate of increase of HF in the lower mesosphere, *Geophys. Res. Lett., 24*, 3217-3220, 1997.

Cunnold, D., H. J. Wang, L. Thomason, J. Zawodny, and J. Logan, SAGE (v5.96) ozone trends in the lower stratosphere, *J. Geophys. Res.*, in press, 1998.

David, S. J., F. J. Murcray, A. Goldman, C. P. Rinsland, and D. G. Murcray, The effect of the Mt. Pinatubo aerosol on the $HNO_3$ column over Mauna Loa, Hawaii, *Geophys. Res. Lett., 21*, 1003-1006, 1994.

Dessler, A. E., E. M. Weinstock, E. J. Hintsa, J. G. Anderson, C. R. Webster, R. D. May, J. W. Elkins, and G. S. Dutton, An examination of the total hydrogen budget of the lower stratosphere, *Geophys. Res. Lett., 21*, 2563-2566, 1994.

Dlugokencky, E. J., L. P. Steele, P. M. Lang, and K. A. Masarie, The growth rate and distribution of atmospheric methane, *J. Geophys. Res., 99*, 17,021-17,043, 1994.

Dlugokencky, E. J., K. A. Masarie, P. M. Lang, and P. P. Tans, Continuing decline in the growth rate of atmospheric methane burden, *Nature, 393*, 447-450, 1998.

Efron, B., and R. J. Tibshirani, *An Introduction to the Bootstrap*, vol. 57, *Monographs on Statistics and Applied Probability*, 436 pp., Chapman and Hall, New York, 1993.

Eluszkiewicz, J., D. Crisp, R. G. Grainger, A. Lambert, A. E. Roche, J. B. Kumer, and J. L. Mergenthaler, Sensitivity of the residual circulation diagnosed from UARS data to the uncertainties in the input fields and the inclusion of aerosols, *J. Atmos. Sci., 54*, 1739-1757, 1997.

Evans, S. J., R. Toumi, J. E. Harries, M. P. Chipperfield, and J. M. Russell III, Trends in stratospheric humidity and the sensitivity of ozone to these trends, *J. Geophys. Res., 103*, 8715-8725, 1998.

Froidevaux, L., et al., Validation of UARS Microwave Limb Sounder ozone measurements, *J. Geophys. Res., 101*, 10,017-10,060, 1996.

Gordley, L. L., et al., Validation of nitric oxide and nitrogen dioxide measurements made by the Halogen Occultation Experiment for UARS platform, *J. Geophys. Res., 101*, 10,241-10,266, 1996.

Hall, T. M., and D. W. Waugh, Timescales for the stratospheric circulation derived from tracers, *J. Geophys. Res., 102*, 8991-9001, 1997.

Harries, J. E., et al., Validation of measurements of water vapor from the Halogen Occultation Experiment (HALOE), *J. Geophys. Res., 101*, 10,205-10,216, 1996.

Koike, M., N. B. Jones, W. A. Matthews, P. V. Johnston, R. L. McKenzie, D. Kinnison, and J. Rodriguez, Impact of Pinatubo aerosols on the partitioning between $NO_2$ and $HNO_3$, *Geophys. Res. Lett., 21*, 597-600, 1994.

Kutzbach, J. E., Large-scale features of monthly mean Northern

Hemisphere anomaly maps of sea-level pressure, *Mon. Weather Rev., 98*, 708-716, 1970.

Lary, D. J., and R. Toumi, Halogen-catalyzed methane oxidation, *J. Geophys. Res., 102*, 23,421-23,428, 1997.

Luo, M., R. J. Cicerone, J. M. Russell III, and T.Y.W. Huang, Observations of stratospheric hydrogen fluoride by the Halogen Occultation Experiment (HALOE), *J. Geophys. Res., 99*, 16,691-16,705, 1994.

Luo, M. R., J. M. Russell III, and T.Y.W. Huang, HALOE observations of the quasi-biennial oscillation and the effects of Pinatubo aerosols in the tropical stratosphere, *J. Geophys. Res., 102*, 19,187-19,198, 1997.

McPeters, R. D., S. M. Hollandsworth, L. E. Flynn, J. R. Herman, and C. J. Seftor, Long-term ozone trends derived from the 16-year combined Nimbus 7/Meteor 3 TOMS Version 7 record, *Geophys. Res. Lett., 23*, 3699-3702, 1996.

Montzka, S., J. H. Butler, R. C. Myers, T. M. Thompson, T. H. Swanson, A. D. Clarke, L. T. Lock, and J. W. Elkins, Decline in the tropospheric abundance of halogen from halocarbons: Implications for stratospheric ozone depletion, *Science, 272*, 1318-1322, 1996.

Mote, P. W., et al., An atmospheric tape recorder: The imprint of tropical tropopause temperatures on stratospheric water vapor, *J. Geophys. Res., 101*, 3989-4006, 1996.

Nedoluha, G. E., R. M. Bevilacqua, R. M. Gomez, D. E. Siskind, and B. C. Hicks, Increases in middle atmospheric water vapor as observed by the Halogen Occultation Experiment and the ground-based Water Vapor Millimeter-Wave Spectrometer from 1991 to 1997, *J. Geophys. Res., 103*, 3531-3543, 1998a.

Nedoluha, G. E., D. E. Siskind, J. T. Bacmeister, R. M. Bevilacqua, and J. M. Russell III, Changes in upper stratospheric $CH_4$ and $NO_2$ as measured by HALOE and implications for changes in transport, *Geophys. Res. Lett., 25*, 987-990, 1998b.

Nevison, C. D., S. Solomon, and J. M. Russell III, Nighttime formation of $N_2O_5$ inferred from the Halogen Occultation Experiment sunset/sunrise $NO_x$ ratios, *J. Geophys. Res., 101*, 6741-6748, 1996.

Oltmans, S. J., and D. J. Hofmann, Increase in lower-stratospheric water vapor at a midlatitude Northern Hemisphere site from 1981 to 1994, *Nature, 374*, 146-149, 1995.

Osterman, G. B., R. J. Salawitch, B. Sen, G. C. Toon, R. A. Stachnik, H. M. Pickett, J. J. Margitan, J. F. Blavier, and D. B. Peterson, Balloon-borne measurements of stratospheric radicals and their precursors: Implications for the production and loss of ozone, *Geophys. Res. Lett., 24*, 1107-1110, 1997.

Park, J. H., et al., Validation of Halogen Occultation Experiment $CH_4$ measurements from the UARS, *J. Geophys. Res., 101*, 10,183-10,203, 1996.

Randel, W. J., F. Wu, J. M. Russell III, J. W. Waters, and L. Froidevaux, Ozone and temperature changes in the stratosphere following the eruption of Mt. Pinatubo, *J. Geophys. Res., 100*, 16,753-16,764, 1995.

Randel, W. J., F. Wu, J. M. Russell III, A. Roche, and J. W. Waters, Seasonal cycles and QBO variations in stratospheric $CH_4$ and $H_2O$ observed in UARS HALOE data, *J. Atmos. Sci., 55*, 163-185, 1998.

Reber, C. A., The Upper Atmosphere Research Satellite (UARS), *Geophys. Res. Lett., 20*, 1215-1218, 1993.

Remsberg, E. E., J. M. Russell III, L. L. Gordley, J. C. Gille, and P. L. Bailey, Implications of stratospheric water vapor distributions as determined from the Nimbus 7 LIMS Experiment, *J. Atmos. Sci., 41*, 2934-2945, 1984.

Remsberg, E. E., P. P. Bhatt, and J. M. Russell III, Estimates of the water vapor budget of the stratosphere from UARS HALOE data, *J. Geophys. Res., 101*, 6749-6766, 1996.

Rosenfield, J. E., D. B. Considine, P. E. Meade, J. T. Bacmeister, C. H. Jackman, and M. R. Schoeberl, Stratospheric effects of Mount Pinatubo aerosol studied with a coupled two-dimensional model, *J. Geophys. Res., 102*, 3649-3670, 1997.

Russell III, J. M., et al., The halogen occultation experiment, *J. Geophys. Res., 98*, 10,777-10,797, 1993.

Russell III, J. M., M. Luo, R. J. Cicerone, and L. E. Deaver, Satellite confirmation of the dominance of chlorofluorocarbons in the global stratospheric chlorine budget, *Nature, 379*, 526-529, 1996a.

Russell III, J. M., et al., Validation of hydrogen chloride measurements made by the Halogen Occultation Experiment from the UARS platform, *J. Geophys. Res., 101*, 10,151-10,162, 1996b.

Russell III, J. M., et al., Validation of hydrogen fluoride measurements made by the Halogen Occultation Experiment from the UARS platform, *J. Geophys. Res., 101*, 10,163-10,174, 1996c.

Siskind, D. E., L. Froidevaux, J. M. Russell III, and J. Lean, Implications of upper stratospheric trace constituent changes observed by HALOE for $O_3$ and ClO from 1992 to 1995, *Geophys. Res. Lett., 25*, 3513-3516, 1998.

Thomason, L. W., L. R. Poole, and T. Deshler, A global climatology of stratospheric aerosol surface area density deduced from Stratospheric Aerosol and Gas Experiment II measurements: 1984-1994, *J. Geophys. Res., 102*, 8967-8976, 1997.

Wallace, J. M., C. Smith, and C. S. Bretherton, Singular value decomposition of wintertime sea surface temperature and 500-mb height anomalies, *J. Clim., 5*, 561-576, 1992.

Waters, J. W., et al., Validation of UARS Microwave Limb Sounder ClO measurements, *J. Geophys. Res., 101*, 10,091-10,127, 1996.

Waugh, D. W., et al., Three-dimensional simulations of long-lived tracers using winds from MACCM2, *J. Geophys. Res., 102*, 21,493-21,513, 1997.

World Meteorological Organization, Report of the International Ozone Trends Panel, *WMO Report 18*, Geneva, Switzerland, 1989.

World Meteorological Organization (WMO), Assessment of trends in the vertical distribution of ozone, edited by N. Harris, R. Hudson, and C. Phillips, *Rep. 43*, Ozone Res. and Monit. Proj., Geneva, May 1998.

World Meteorological Organization (WMO), Scientific Assessment of Ozone Depletion: 1998, *WMO Report 44*, Geneva, Switzerland, 1998.

W. J. Randel and F. Wu, National Center for Atmospheric Research, P. O. Box 3000, Boulder, CO 80307. (e-mail: randel@ucar.edu; wuf@ucar.edu)

J. M. Russell, Hampton University, Hampton, VA 23668. (e-mail: jmr@hamptonu.edu)

J. Waters, Jet Propulsion Laboratory, Pasadena, CA 91109. (e-mail: joe@mls.jpl.nasa.gov)

(Received June 2, 1998; revised September 28, 1998; accepted September 30, 1998.)